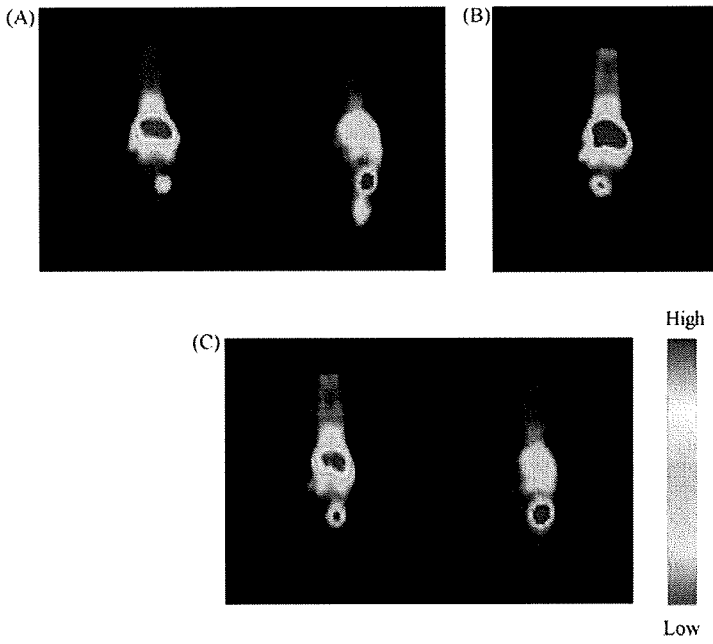

Fig. 2. Imaging of biodistribution of PEGylated liposomes with PPIS. Whole-body imaging of biodistribution of [^{18}F]-labeled PEGylated liposomes in BALB/c mice pretreated with PBS (A), PEGylated liposomes (B), or PEG–Dox liposomes (C) was performed by use of PPIS. Data were integrated into 1–30 (left image) or 31–60 min (right image) periods following the injection of [^{18}F]-labeled PEGylated liposomes.

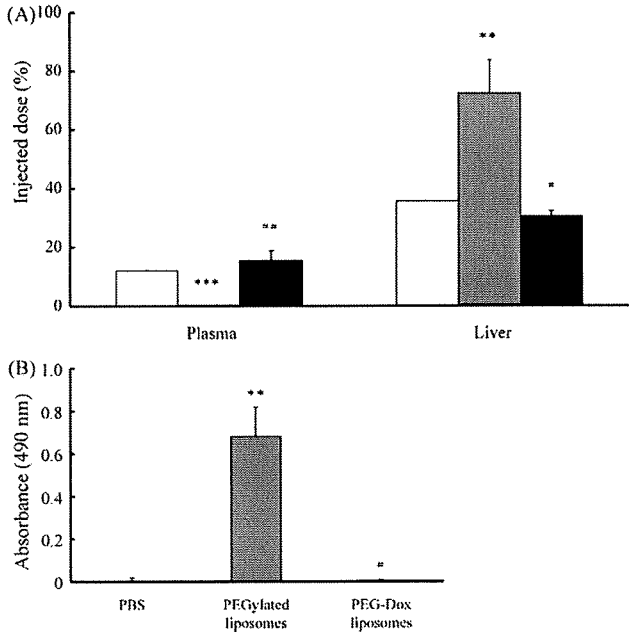

Fig. 3. Induction of the ABC phenomenon in BALB/c *nu/nu* mice. BALB/c *nu/nu* mice were intravenously injected with PBS, PEGylated liposomes or PEG–Dox liposomes. (A) Biodistribution of the test-dose ^{3}H-labeled PEGylated liposomes: 3 days after the pretreatment, ^{3}H-labeled PEGylated liposomes were intravenously injected into these mice (5 μmol DPPC dosage/kg). Twenty-four hours after the second injection, the mice were sacrificed, and the radioactivity in the plasma and each organ (only liver data shown) was determined. Data (n = 5) are presented as a percentage of the injected dose per tissue and S.D. and (B) anti-PEG IgM in the serum collected at day 3 after the pretreatment. Each value represents the mean ± S.D. of 3 separate experiments. Data are presented for PBS (open bar), PEGylated liposomes (gray bar), and PEG–Dox liposomes (closed bar). Significant differences: $^{**}p < 0.01$ and $^{***}p < 0.001$ *vs.* PBS; $^{\#\#}p < 0.01$ and $^{\#}p < 0.001$ *vs.* PEGylated liposomes.

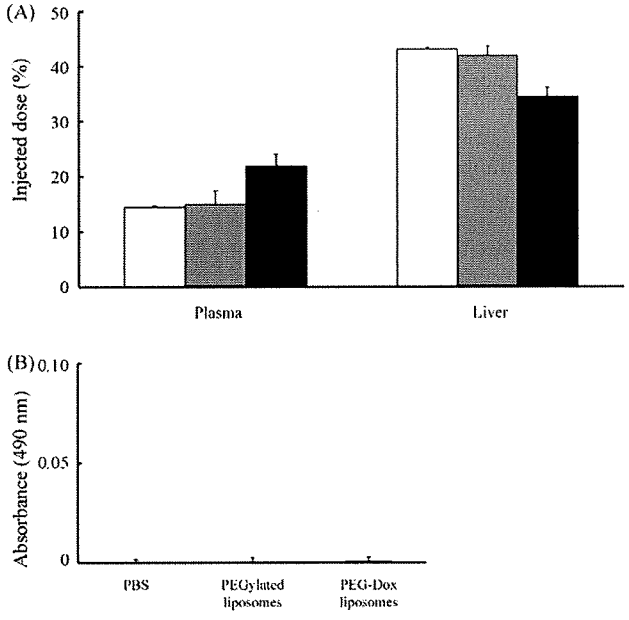

Fig. 4. No induction of the ABC phenomenon in BALB/c SCID mice. BALB/c SCID mice were intravenously injected with PBS, PEGylated liposomes or PEG–Dox liposomes. (A) Biodistribution of the test-dose ^{3}H-labeled PEGylated liposomes: 3 days after the pretreatment, ^{3}H-labeled PEGylated liposomes were administered via a tail vein (5 μmol DPPC dosage/kg). Twenty-four hours after the second injection, these mice were sacrificed; and the radioactivity in the plasma and each organ was then determined. Data (n = 5) are presented as a percentage of the injected dose per tissue and S.D. and (B) anti-PEG IgM in the serum collected at day 3 after the pretreatment. Each value represents the mean ± S.D. of 3 separate experiments. Data are presented for PBS (open bar), PEGylated liposomes (gray bar), and PEG–Dox (closed bar).

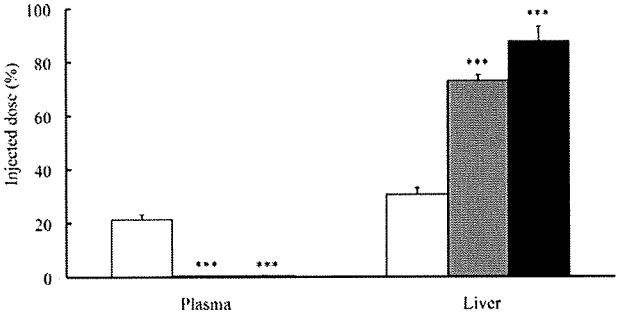

Fig. 5. Induction of the ABC phenomenon with non-PEGylated liposomes. BALB/c mice were intravenously injected with PBS, PEGylated liposomes, or non-PEGylated liposomes. Three days after pretreatment, ^{3}H-labeled PEGylated liposomes were administered via a tail vein. Twenty-four hours after the second injection, these mice were sacrificed; and the radioactivity in the plasma and each organ was then determined ($n = 5$). Data are presented as a percentage of the injected dose per tissue and S.D. Data are presented for PBS (open bar), PEGylated liposomes (gray bar), and non-PEGylated liposomes (closed bar), respectively. Significant differences: ***$p < 0.001$ *vs.* PBS.

3.5. Low specificity in the induction of the ABC phenomenon

We next focused on the specificity in the induction of the ABC phenomenon since T cell-independent B cell response against thymus-independent type 2 (TI-2) antigen might trigger this phenomenon. To elucidate the specificity in the induction of the ABC phenomenon, we preadministered non-PEGylated liposomes to BALB/c mice, and then studied the biodistribution of the test-dose PEGylated liposomes. As shown in Fig. 5, the hepatic uptake and the clearance from bloodstream of the test-dose PEGylated liposomes were increased dramatically in the mice pretreated with non-PEGylated liposomes, as in the case of pretreatment with PEGylated liposomes. This indicates that the ABC phenomenon was thus induced regardless of modification of the liposomes with PEG chains.

3.6. Time-dependency of anti-PEG IgM antibody production

We next determined the time-dependency of the production of anti-PEG IgM antibody in BALB/c mice. The amount of anti-PEG IgM antibody was determined at days 1, 3, 7, 11, 14, 21 and 27 after pretreatment with PEGylated liposomes, PEG–Dox liposomes, or PBS. Anti-PEG IgM antibody production reached maximum level about 3 days after the administration of PEGylated liposomes (Fig. 6). This transient increase in IgM antibody like T cell-independent B cell response was observed in this experiment. On the contrary, the PBS and PEG–Dox liposomes groups showed little production of anti-PEG IgM antibody.

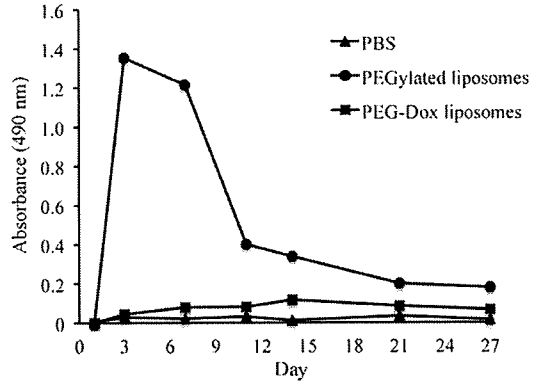

Fig. 6. Time-course of anti-PEG IgM antibody production. BALB/c mice were intravenously injected with PBS, PEGylated liposomes or PEG–Dox liposomes. At days 1, 3, 7, 11, 14, 21, and 27 after the injection, serum samples were collected. Anti-PEG IgM antibody was then detected by ELISA.

4. Discussion

The ABC phenomenon implies caution about the pharmacokinetics of nanoparticles in the case of repeated injection of nanomedicines, especially in the clinical setting. Thus, elucidating the mechanism of the ABC phenomenon is important for the development of DDS (drug delivery system) drugs. In this study, we determined the biodistribution of test-dose PEGylated liposomes in mice preadministered PEG–Dox liposomes or a mixture of free Dox and "empty" PEGylated liposomes. We and Laverman et al. previously reported that the ABC phenomenon was not induced when the rats were pretreated with PEG–Dox liposomes (Ishida et al., 2006a,b,c; Laverman et al., 2001). These reports indicated that preadministration of PEG–Dox liposomes could abolish the induction of the ABC phenomenon, although the effect of the mixture of free Dox and "empty" PEGylated liposomes has not been clarified. The production of anti-PEG IgM antibody was increased by the administration of the mixture of free Dox and "empty" PEGylated liposomes in a manner similar to that of PEGylated liposomes, but no increase was seen with PEG–Dox liposomes. These data suggest the importance of Dox delivery to immune cells by PEGylated liposomes, and indicate that Dox encapsulated in the liposomes was delivered to the immune cells responsible for the ABC phenomenon. And then, Dox that had been taken up into the immune cells could induce apoptosis of them, resulting in no induction of the IgM antibody against PEGylated liposomes and ABC phenomenon. In general, free Dox causes adverse reactions such as leucopenia and cardiotoxicity. Liposomal Dox was developed to reduce these side effects, which could significantly increase the tolerable dosage (O'brien et al., 2004). If the induction of the ABC phenomenon was canceled by a non-specific effect of Dox, the mixture of free Dox and "empty" PEGylated liposomes would have abolished the induction of the phenomenon. Accordingly, we conclude that the encapsulation of cytotoxic agents in PEGylated liposomes prevents the induction of the ABC phenomenon.

The ABC phenomenon was observed in the BALB/c *nu/nu* mice, but not in the BALB/c SCID mice. In addition, production of anti-PEG IgM antibody was increased by the injection of PEGylated liposomes in BALB/c *nu/nu* mice but not in BALB/c SCID mice at all. These results suggest that the induction of ABC phenomenon is independent of the T cells, but dependent on B cells. On the other hand, the phenomenon was also induced by the preadministration of non-PEGylated liposomes, suggesting that the specificity of the IgM antibody would be comparatively low. In this point, we previously reported that the administration of PEGylated liposomes triggered IgM antibody production against both PEG moieties and lipid moieties in rats, although the reactivity of IgM antibody against the latter was not so high (Wang et al., 2007). Anti-PEG IgM antibody produced by preadministration of PEGylated liposomes was transiently increased and then decreased rapidly. These data suggest that PEGylated liposomes might be recognized as a TI-2 antigen.

In general, most antigens in the natural world are T cell-dependent antigen. In the immune response to them, naïve B cells can differentiate into immunoglobulin-secreting cells or they can seed a germinal center and develop into memory B cells after exposure to a T cell-dependent antigen (Ahmed and Gray, 1996; Liu et al., 1988, 1991). However, there are other type antigens which are composed of repetitive structures such as polysaccharides or lipopolysaccharide derived from bacteria and belong to the TI-2 antigen category. These antigens activate B cells, which then produce antibodies such as IgM and IgG without the interaction with

helper T cells; and these IgM antibodies tend to have low affinity (Beringue et al., 2000). TI-2 responses are characterized by early B cell proliferation in all splenic compartments and differentiation into antibody-producing plasma cells starting at day 3 after immunization, but the number of plasma cells falls markedly during the second week after immunization (Garcia De Vinuesa et al., 1999). These TI-2 antigens induce only limited isotype switching and do not induce memory B cells (Beringue et al., 2000). In addition, B cells respond against TI-2 antigens and profoundly participate in the response of complements (Zandvoort and Timens, 2002). It is therefore considered that when PEGylated liposomes enter into the bloodstream, complement components may bind to the liposomal surface and activate B cells to secrete IgM antibodies such as anti-PEG IgM antibody. Marginal zone B (MZ-B) cells in the spleen and B-1B cells in the intraperitoneal cavity play a central role in the immune response against TI-2 antigen (Martin and Kearney, 2002). Since we have already reported that the phenomenon was not induced in rats that had had their spleens removed (Ishida et al., 2006a,b,c), we hypothesize that MZ-B cells recognize PEGylated liposomes as a TI-2 antigen and secrete anti-PEG IgM antibody. It appears that anti-PEG IgM antibody binds to the test-dose PEGylated liposomes and makes complexes with complement components. Then, these complexes accumulate in the liver, resulting in the rapid clearance of PEGylated liposomes.

Our present findings strongly suggest that PEGylated liposomes and conventional liposomes without PEG modification are recognized as TI-2 antigens and that the induction of the ABC phenomenon is related to a T cell-independent B cell response.

5. Conclusion

This study revealed that the ABC phenomenon occurred in BALB/c *nu/nu* mice, but not in BALB/c SCID mice. Anti-IgM antibody production, possibly derived from a T cell-independent B cell response, would be essential for the induction of the phenomenon. We anticipate that the elucidation of the ABC phenomenon will be helpful for the development of future DDS formulations.

Acknowledgments

This research was supported by global COE program. We thank Philip Hawke at the University of Shizuoka for helpful advice in writing the manuscript.

References

Ahmed, R., Gray, D., 1996. Immunological memory and protective immunity: understanding their relation. Science 272, 54–60.

Allen, T.M., 1994. Long-circulating (sterically stabilized) liposomes for targeted drug delivery. Trends Pharmacol. Sci. 15, 215–220.

Beringue, V., Demoy, M., Lasmezas, C.I., Gouritin, B., Weingarten, C., Deslys, J.P., Andreux, J.P., Couvreur, P., Dormont, D., 2000. Role of spleen macrophages in the clearance of scrapie agent early in pathogenesis. J. Pathol. 190, 495–502.

Berry, G., Billingham, M., Alderman, E., Richardson, P., Torti, F., Lum, B., Patek, A., Martin, F.J., 1998. The use of cardiac biopsy to demonstrate reduced cardiotoxicity in AIDS Kaposi's sarcoma patients treated with pegylated liposomal doxorubicin. Ann. Oncol. 9, 711–716.

Dams, E.T., Laverman, P., Oyen, W.J., Storm, G., Scherphof, G.L., Van Der Meer, J.W., Corstens, F.H., Boerman, O.C., 2000. Accelerated blood clearance and altered biodistribution of repeated injections of sterically stabilized liposomes. J. Pharmacol. Exp. Ther. 292, 1071–1079.

Garcia De Vinuesa, C., O'leary, P., Sze, D.M., Toellner, K.M., Maclennan, I.C., 1999. T-independent type 2 antigens induce B cell proliferation in multiple splenic sites, but exponential growth is confined to extrafollicular foci. Eur. J. Immunol. 29, 1314–1323.

Ishida, T., Atobe, K., Wang, X., Kiwada, H., 2006a. Accelerated blood clearance of PEGylated liposomes upon repeated injections: effect of doxorubicin-encapsulation and high-dose first injection. J. Control. Release 115, 251–258.

Ishida, T., Harada, M., Wang, X.Y., Ichihara, M., Irimura, K., Kiwada, H., 2005. Accelerated blood clearance of PEGylated liposomes following preceding liposome injection: effects of lipid dose and PEG surface-density and chain length of the first-dose liposomes. J. Control. Release 105, 305–317.

Ishida, T., Ichihara, M., Wang, X., Kiwada, H., 2006b. Spleen plays an important role in the induction of accelerated blood clearance of PEGylated liposomes. J. Control. Release 115, 243–250.

Ishida, T., Ichihara, M., Wang, X., Yamamoto, K., Kimura, J., Majima, E., Kiwada, H., 2006c. Injection of PEGylated liposomes in rats elicits PEG-specific IgM, which is responsible for rapid elimination of a second dose of PEGylated liposomes. J. Control. Release 112, 15–25.

Ishida, T., Maeda, R., Ichihara, M., Irimura, K., Kiwada, H., 2003a. Accelerated clearance of PEGylated liposomes in rats after repeated injections. J. Control. Release 88, 35–42.

Ishida, T., Masuda, K., Ichikawa, T., Ichihara, M., Irimura, K., Kiwada, H., 2003b. Accelerated clearance of a second injection of PEGylated liposomes in mice. Int. J. Pharm. 255, 167–174.

Ishida, T., Wang, X., Shimizu, T., Nawata, K., Kiwada, H., 2007. PEGylated liposomes elicit an anti-PEG IgM response in a T cell-independent manner. J. Control. Release 122, 349–355.

Koide, H., Asai, T., Hatanaka, K., Urakami, T., Ishii, T., Kenjo, E., Nishihara, M., Yokoyama, M., Ishida, T., Kiwada, H., Oku, N., 2008. Particle size-dependent triggering of accelerated blood clearance phenomenon. Int. J. Pharm. 362, 197–200.

Lasic, D.D., Martin, F.J., Gabizon, A., Huang, S.K., Papahadjopoulos, D., 1991. Sterically stabilized liposomes: a hypothesis on the molecular origin of the extended circulation times. Biochim. Biophys. Acta 1070, 187–192.

Laverman, P., Carstens, M.G., Boerman, O.C., Dams, E.T., Oyen, W.J., Van Rooijen, N., Corstens, F.H., Storm, G., 2001. Factors affecting the accelerated blood clearance of polyethylene glycol-liposomes upon repeated injection. J. Pharmacol. Exp. Ther. 298, 607–612.

Liu, Y.J., Oldfield, S., Maclennan, I.C., 1988. Memory B cells in T cell-dependent antibody responses colonize the splenic marginal zones. Eur. J. Immunol. 18, 355–362.

Liu, Y.J., Zhang, J., Lane, P.J., Chan, E.Y., Maclennan, I.C., 1991. Sites of specific B cell activation in primary and secondary responses to T cell-dependent and T cell-independent antigens. Eur. J. Immunol. 21, 2951–2962.

Maeda, H., Wu, J., Sawa, T., Matsumura, Y., Hori, K., 2000. Tumor vascular permeability and the EPR effect in macromolecular therapeutics: a review. J. Control. Release 65, 271–284.

Maeda, N., Takeuchi, Y., Takada, M., Sadzuka, Y., Namba, Y., Oku, N., 2004. Anti-neovascular therapy by use of tumor neovasculature-targeted long-circulating liposome. J. Control. Release 100, 41–52.

Martin, F., Kearney, J.F., 2002. Marginal-zone B cells. Nat. Rev. Immunol. 2, 323–335.

Muggia, F.M., 1999. Doxorubicin-polymer conjugates: further demonstration of the concept of enhanced permeability and retention. Clin. Cancer Res. 5, 7–8.

O'brien, M., Wigler, N., Inbar, M., Rosso, R., Grischke, E., Santoro, A., Catane, R., Kieback, D., Tomczak, P., Ackland, S., Orlandi, F., Mellars, L., Alland, L., Tendler, C., Group Caelyx Breast Cancer Study, 2004. Reduced cardiotoxicity and comparable efficacy in a phase III trial of pegylated liposomal doxorubicin HCl (CAELYX/Doxil) versus conventional doxorubicin for first-line treatment of metastatic breast cancer. Ann. Oncol. 15, 440–449.

Oku, N., Doi, K., Namba, Y., Okada, S., 1994. Therapeutic effect of adriamycin encapsulated in long-circulating liposomes on Meth-A-sarcoma-bearing mice. Int. J. Cancer 58, 415–419.

Torchilin, V.P., Omelyanenko, V.G., Papisov, M.I., Bogdanov Jr., A.A., Trubetskoy, V.S., Herron, J.N., Gentry, C.A., 1994. Poly(ethylene glycol) on the liposome surface: on the mechanism of polymer-coated liposome longevity. Biochim. Biophys. Acta 1195, 11–20.

Urakami, T., Akai, S., Katayama, Y., Harada, N., Tsukada, H., Oku, N., 2007. Novel amphiphilic probes for [18F]-radiolabeling preformed liposomes and determination of liposomal trafficking by positron emission tomography. J. Med. Chem. 50, 6454–6457.

Van Rooijen, N., Van Nieuwmegen, R., 1980. Liposomes in immunology: multilamellar phosphatidylcholine liposomes as a simple, biodegradable and harmless adjuvant without any immunogenic activity of its own. Immunol. Commun. 9, 243–256.

Wang, X., Ishida, T., Kiwada, H., 2007. Anti-PEG IgM elicited by injection of liposomes is involved in the enhanced blood clearance of a subsequent dose of PEGylated liposomes. J. Control. Release 119, 236–244.

Zandvoort, A., Timens, W., 2002. The dual function of the splenic marginal zone: essential for initiation of anti-TI-2 responses but also vital in the general first-line defense against blood-borne antigens. Clin. Exp. Immunol. 130, 4–11.

BRAIN RESEARCH 1321 (2010) 164–168

available at www.sciencedirect.com

ScienceDirect

www.elsevier.com/locate/brainres

BRAIN RESEARCH

Research Report

Accumulation of macromolecules in brain parenchyma in acute phase of cerebral infarction/reperfusion

*Takayuki Ishii, Tomohiro Asai, Takeo Urakami, Naoto Oku**

Department of Medical Biochemistry and Global COE, School of Pharmaceutical Sciences, University of Shizuoka, 52-1 Yada, Suruga-ku, Shizuoka 422-8526, Japan

ARTICLE INFO

Article history:
Accepted 13 January 2010
Available online 21 January 2010

Keywords:
Stroke
Reperfusion injury
BBB
t-MCAO
Macromolecule

ABSTRACT

Ischemia–reperfusion injury is induced by recovery of blood flow after ischemia. This phenomenon is a main cause of ischemic brain injury. The integrity of the blood–brain barrier (BBB) fails after cerebral ischemia and reperfusion. Further elucidation of this phenomenon promotes to develop treatment strategies for ischemia–reperfusion injury. In the present study, we attempted to examine the time-dependent change of ischemia–reperfusion injury in relation to BBB disorders at acute phase in a transient middle cerebral artery occlusion (t-MCAO) model rat as a cerebral infarction and reperfusion model. Brain cell damage after the reperfusion was assessed by 2, 3, 5-triphenyltetrazolium chloride (TTC) staining. To clarify a time-dependent change of the integrity of BBB, fluorescein isothiocyanate (FITC)-dextran (150 kDa) was injected intravenously into t-MCAO rats, and time-dependent localization of FITC-dextran was monitored in ex vivo. As a result, obvious brain damage was firstly observed at 3 h after reperfusion following 1 h of MCAO. In contrast, the leakage of FITC-dextran from cerebral vessels was observed immediately after the reperfusion. The present data suggest that the integrity of BBB failed prior to the occurrence of serious brain damage induced by ischemia–reperfusion, and that macromolecules such as water-soluble polymers and proteins which cannot pass through the BBB under normal condition would reach brain parenchyma at early stage after reperfusion. These findings would be useful to establish a novel treatment strategy for reperfusion injury after cerebral infarction.

1. Introduction

The BBB strictly limits material exchange in the brain, which makes drug delivery to the brain tissue difficult. However, it is known that the integrity of the BBB fails after cerebral ischemia and reperfusion, resulting in increase in cerebrovascular permeability (Yang and Betz, 1994). Several factors including reactive oxygen species, matrix metalloprotease (MMP)-2, and -9, vascular endothelial growth factor (VEGF) are considered to be related with increase in permeability by change of cerebral vascular tonus and disruption of basement membrane after reperfusion following cerebral stroke (Rosenberg et al., 1998; Zhang et al., 2002).

In the treatment of cerebral stroke, ischemic penumbra is one of the most important concepts (Lo, 2008). It is defined as ischemic but still viable cerebral tissue. This area recovers if cerebral blood flow is rapidly improved. The aim of treatment for acute phase of cerebral stroke is to recover cerebral blood

* *Corresponding author.* Fax: +81 54 264 5705.
E-mail address: oku@u-shizuoka-ken.ac.jp (N. Oku).

0006-8993/$ – see front matter © 2010 Elsevier B.V. All rights reserved.
doi:10.1016/j.brainres.2010.01.039

flow and to revive the function of neuronal cells in the penumbra. However, many deleterious mediators are upregulated and injure brain tissue by reperfusion after ischemia. For example, reactive oxygen species such as hydrogen peroxide, hydroxyl radicals and superoxide are produced by reperfusion following brain ischemia (Kontos, 2001). They cause cerebral vasodilatation, resulting in brain tissue injury. In fact, α-amino-3-hydroxy-5-methylisoxasolepropionic acid (AMPA) is known to mediate superoxide generation, and the inhibition of AMPA receptor improves ischemic outcome (Erdo et al., 2005). Many other pathways are also involved in secondary brain lesion after cerebral infarction (Cunningham et al., 2005; Huang et al., 2006). This cerebral ischemia–reperfusion injury substantially influences prognosis and mortality of patients treated with thrombolytic agents for cerebral infarct therapy. Therefore, improvement of ischemia–reperfusion injury is essential for the treatment of cerebral ischemia and required to protect a cerebral neuronal cell. Although mechanisms of reperfusion injury after cerebral infarction have been widely studied in the world, clinically available drug at present is only Radicut® (edaravone), a free radical scavenger, for cerebral neuroprotection during cerebral ischemia/reperfusion (Yoshida et al., 2006).

In the case of acute disease such as cerebral infarction, therapeutic time window (TTW) is an important concept. It is defined as the promising time to achieve therapeutic efficacy. For example, tissue plasminogen activator (t-PA), a thrombolytic agent, for treatment of cerebral stroke is decided to inject within 3 h because it has prospects of worsening symptoms more than 3 h after ischemia (Marler and Goldstein, 2003).

t-MCAO model rats by a filament method are used to the study of ischemia–reperfusion injury after focal ischemia (Nagasawa and Kogure, 1989). This method can make a stable cerebral occlusion model using a nylon uniformly coated with silicon. In addition, reperfusion is induced easily by pulling the thread out of the artery. Since this model needs no materials such as t-PA to induce reperfusion, the influences of reperfusion can be observed directly without considering superfluous factors.

Macromolecules with biocompatibility and size above 40 kDa possess long-circulating characteristic in bloodstream, and tend to localize at the site where the vascular permeability is increased (Seymour et al., 1995). In fact, vascular permeability is known to increase at inflammatory site, and a dendritic polymer complexed with ibuprofen is reported to localized and retained at the inflammatory site resulting in a high anti-inflammatory effect (Kannan et al., 2004; Svenson, 2009). Moreover, in myocardial ischemia/reperfusion that shows similar pathological event to cerebral ischemia/reperfusion, macromolecular agents accumulated in the infarction zone at early stage by vascular permeability increase (Lukyanov et al., 2004). However it isn't known that time-dependent change in the extent of diffusion of macromolecules into brain tissue by disruption of the BBB after cerebral ischemia/reperfusion in acute phase.

In the present study, we attempted to clarify the time-dependent relationship between ischemia–reperfusion damage and localization of macromolecules by increasing BBB permeability in t-MCAO model rats for the purpose of the determination of effective term for the treatment of reperfusion injury using macromolecular drugs or drugs in macromolecules.

2. Results

2.1. *Brain damage assessment*

The time-dependent change of ischemia/reperfusion damage was assessed by TTC staining. A ratio between right and left hemisphere section areas represents brain edema. When this ratio significantly exceeds 1, edema is induced on the side of the occlusion. Fig. 1 shows representative photographs of the brain damage in the t-MCAO rats. Total brain slice areas and damaged ones are calculated by Image J, and their mean values are shown in Table 1. The damage of the brain tissue was firstly observed in the section of the MCA at 3 h after the reperfusion. At 6 h after the reperfusion, the damage was observed more broadly than at 3 h, and the cell death progressed to cerebral cortex. Moreover, the most widespread damage was observed at 24 h after the reperfusion. Similarly, the brain edema was firstly observed at 3 h after the reperfusion. However, significant cerebral damage was not observed until 3 h after the reperfusion.

2.2. *Leakage of FITC-dextran*

Time course of the change in cerebral blood vessel permeability after reperfusion in the t-MCAO rat were monitored by the leakage of FITC-dextran with in vivo imaging system. Fig. 2 shows the leakage of FITC-dextran into brain parenchyma at 1 h after the administration. Table 2 shows average of total photon counts obtained from five rats at each time. Interestingly, the leakage of the FITC-dextran from cerebral vessels was observed immediately after the reperfusion in the t-MCAO rat model. This leakage was observed up to 6 h but not at 24 h after the reperfusion. The FITC-dextran localization in brain tissue became broadly as time advances within 3 h. However, the fluorescence intensity was diminished at 6 h compared with that at 3 h.

In the present study, we did not use the same slices in both TTC staining and FITC imaging due to the technical limitation. However the slices were obtained essentially by the same procedure except the injection of FITC-dextran in the latter experiment. Therefore, both TTC staining and FITC imaging would be comparable.

3. Discussion

In the present study, the reperfusion was performed by withdrawing the filament at 1 h after the occlusion using t-MCAO model rats. Although nerve cells suspend electrical activity under ischemic condition, their life is maintained for a few hours because of conservation of ion gradient and cellular membrane pump function (Back, 1998). Therefore, the damage observed in the present study could be mainly derived from reperfusion. Taken together, most of the penumbra area might be protected from death by restoration of blood flow if a treatment for neuroprotection is performed within therapeutic time window.

Cells death of the core infarct area arises predominantly from necrosis, whereas cell death of penumbra area is caused

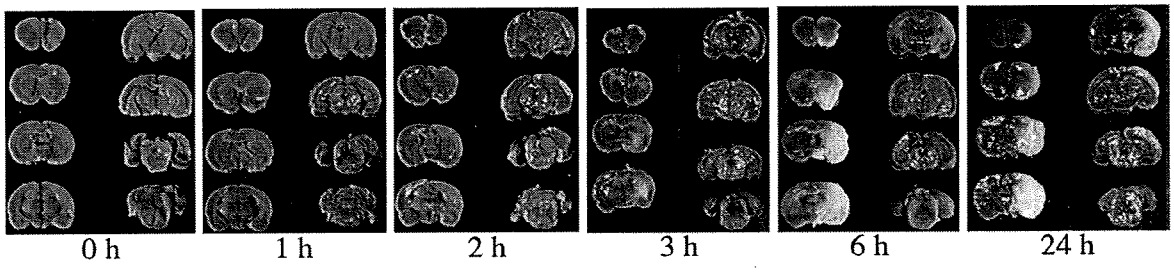

Fig. 1 – Photographs of brain sections prepared from the t-MCAO model rats. The damaged regions were visualized by TTC staining after a 1 h-infarct following 0, 1, 2, 3, 6 or 24 h reperfusion. White areas show the damaged regions and red areas show surviving regions.

mainly by apoptosis following cerebral ischemia (Dirnagl et al., 1999; Lopez-Sanchez et al., 2007; Xu et al., 2006). Therefore, an antiapoptotic agent would protect neuronal cells and attenuate reperfusion injury. In fact, pretreated inhibition of caspase-3 results in decrease of cerebral damage in the penumbra area following 2 h infarct (Zhu et al., 2004). Apoptosis is a key factor improving reperfusion injury, and the detail researches contribute to a new treatment strategy for ischemia–reperfusion injury.

The BBB dysfunction results in cerebral edema, hemorrhage formation and neuronal cell death after cerebral infarction. On the other hand, it permits some drugs that cannot penetrate the BBB in normal condition to reach brain parenchyma. Therefore, it would be one of the promising strategies for improving ischemia–reperfusion injury to delivery agents to brain tissue from cerebral blood flow by increasing BBB permeability. Opening of the BBB has been studied by using many tracers in ischemia/reperfusion. After 2 h occlusion and 3 h reperfusion caused great increase in BBB permeability, which was monitored by the uptake of sucrose (Rosenberg et al., 1998). In the present study, we determined the leakage of macromolecule in more acute phase ischemia/reperfusion. The leakage of FITC-dextran into brain tissue was observed just after the reperfusion in the t-MCAO rat model. These data suggest that tight junction of the BBB fails by reperfusion or 1 h infarct and thus macromolecules such as dextran leak out from bloodstream into the brain tissue. Our findings are consistent with previous reports: For example, a function of myogenic tone, which favors partial vasoconstriction and plays an important role in regulation of cerebrovascular blood flow in response to changes in perfusion pressure, was diminished at early stage after ischemia (Cipolla et al., 1997; Cipolla and Curry, 2002). MMP-2 derived from astrocyte increases at 3 h after reperfusion in the same model rat as the present study (Yang et al., 2007). Therefore, this data suggest that upregulation of MMP-2 is greatly associated with the present result that leakage of FITC-dextran was most broadly at 3 h after reperfusion. Hydroxyl radicals that are one of the most reactivity free radicals greatly increase at immediately after reperfusion in the same model rat as the present study (Kato et al., 2003). Free radicals are related with BBB disruption on how to directly attack cerebral endothelial cells and to mediate MMPs. This report is also associated with the result in the present study. Focusing on the result of 0, 1 and 3 h after reperfusion, fluorescence of FITC-dextran was observed at nearby MCA. In addition, the leakage of FITC-dextran was outspread as time advances. Therefore, BBB disruption progress gradually with time by partial infarct, in this study case is by MCA, after reperfusion.

When neuroprotective agents are delivered to brain tissue for the treatment of ischemia–reperfusion injury by enhanced permeability of a failed BBB, a time widow from appearance of BBB disruption to disappearance of it is very important notion. The integrated data demonstrated that the increase of cerebral vascular permeability from BBB dysfunction was occurred at stages before generation of obvious cerebral cell damage in the t-MCAO model rats. This is important information for the treatment and prevention of reperfusion injury. In general, therapeutic agents for acute phase treatment are beneficial as early injection as possible. However, it is also quite important to know until when do these agents are effective after ischemia–reperfusion. For this reason, here we evaluated the permeability change in BBB and brain damage after ischemia–reperfusion to set TTW in acute phase disease. From the present results, we propose that TTW of reperfusion injury is from immediately after reperfusion up to 3 h. At 6 h after the reperfusion, the brain tissue was broadly impaired, and the leakage of FITC-dextran was diminished, hence suggesting that the possibility to save brain cells is lowered. Obvious cerebral cell death was rarely observed up to 3 h after the reperfusion, and the localization of FITC-dextran was observed earlier than outset of the obvious cerebral cell death. Therefore, some treatments before 3 h after reperfusion are

Table 1 – Time-dependent change of brain injury.

Times after reperfusion	Total volume (cm^3)	Damage volume (cm^3)	Right brain/ left brain
0 h	1.60±0.02	0	1.00±0.00
1 h	1.61±0.02	0	1.01±0.01
2 h	1.61±0.07	0	1.01±0.01
3 h	1.70±0.03	0.05±0.06	1.04±0.02*
6 h	1.72±0.06	0.27±0.07	1.06±0.01**
24 h	1.81±0.05	0.42±0.03	1.12±0.04**

Values are means±SD; $n=5$. Right brain/left brain shows the degree of edema. Statistical differences were calculated by one-way analysis of variance (ANOVA) followed by Dunnett's multiple comparison tests as compared with 0 h after reperfusion group. (*$p<0.05$, **$p<0.01$).

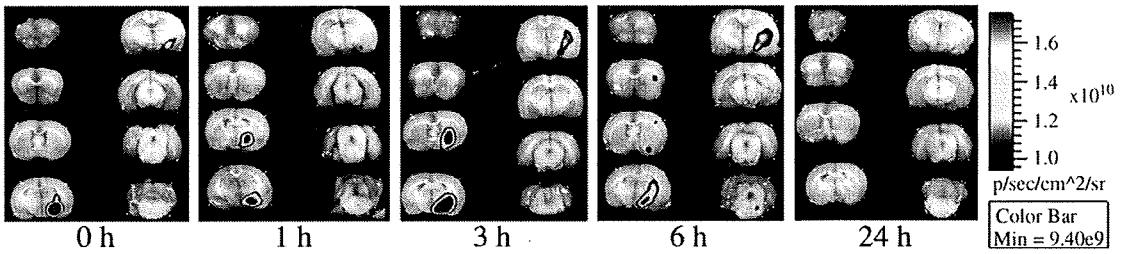

Fig. 2 – The leakage of FITC-dextran in the t-MCAO model rats. Time-dependent change in the integrity of BBB after the reperfusion was monitored by the leakage of FITC-dextran. The t-MCAO rats were injected with FITC-dextran solution (15 mg/ rat *i.v.*). FITC-dextran localized in the brain sections was visualized with IVIS. Bar shows the relative level of fluorescence intensity, ranging from low (blue), to medium (green), to high (yellow, red). This is the representative from five independent animal experiments, all of which demonstrated similar profile of responses.

expected to be significantly effective for the improvement in reperfusion injury.

In conclusion, macromolecules leaked out from blood-stream into brain parenchyma before the obvious cerebral cell death appeared in t-MCAO model rats, and this localization was broadly more than the damage area at 3 h after the reperfusion. The present study suggests that an approach within 3 h after reperfusion is important and promising for the treatment or prevention of reperfusion injury to provide great therapeutic response.

4. Experimental procedures

4.1. *Animal*

Male Wistar rats (8 weeks old) weighing 170–210 g were purchased from Japan SLC Inc. (Shizuoka, Japan). The animals were cared according to the Animal Facility Guidelines of the University of Shizuoka. All animal experiments were approved the by the Animal and Ethics Review Committee of the University of Shizuoka.

4.2. *Preparation of t-MCAO model rat*

Transient middle cerebral artery occlusion (t-MCAO) was induced by inserting a filament into internal carotid artery (Nagasawa and Kogure, 1989). Anesthesia was induced with 3% isoflurane and maintained with 1.5% one during cerebral stroke surgery. Rectal temperature was maintained at 37 °C with heating pad. After a median incision of the neck skin, the right carotid artery, external carotid artery, and internal carotid artery (ICA) were isolated with careful conservation of the vagal nerve. A 4-0 monofilament nylon suture coated with silicon was introduced into the right ICA and advanced into the origin of the MCA. A silk ligated the MCA at side of inserting point. After the operation, the neck was closed and anesthesia was discontinued. Success of the surgery was judged by the appearance of hemiparesis. Reperfusion was performed by withdrawing the filament about 10 mm at 1 h after the occlusion under isoflurane anesthesia in this all study.

Table 2 – Total photon counts of brain sections.

Injection time	Ischemic side ($\times 10^7$)	Nonischemic side ($\times 10^7$)
0 h	4.18±0.32*	3.58±0.16
1 h	5.71±1.28*	3.64±0.69
3 h	6.70±2.47*	3.83±0.57
6 h	4.21±1.11	3.37±0.59
24 h	4.09±0.67	3.83±0.38

Values are means±SD; $n=5$. Accumulation of FITC-dextran in the brain was determined as described in the legend of Fig. 2. Total photon counts were obtained from the IVIS images. Total photon counts of ischemic side are significantly higher than those of nonischemic side at 0, 1 and 3 h. (*$p<0.05$).

4.3. *Brain damage assessment in t-MCAO rat*

The ischemia/reperfusion damage in the t-MCAO rat model was assessed by morphometric analysis of the brain sections stained with 2, 3, 5-triphenyltetrazolium chloride (TTC, Wako Pure Chemical Ind. Ltd., Tokyo, Japan). The brain was dissected at 0, 1, 2, 3, 6 or 24 h after reperfusion and sliced into 2 mm thick coronal sections using a rat brain slicer (Muromachi Kikai, Tokyo, Japan). These sections were stained with 2% TTC in PBS for 30 min at 37 °C. Then, they were fixed in 10% formalin neutral buffer solution. All sections were put in grass slides and photographed with a digital camera (OLYMPUS E-300). We measured the unstained area, the stained area and each hemisphere with an image analysis system (NIH Image J). The damage regions were considered as completely white area. Edema was calculated from a ratio between right and left hemisphere sections area.

4.4. *Leakage of FITC-dextran into brain tissue*

Time-dependent change of the integrity of BBB after reperfusion was determined using fluorescein isothiocyanate (FITC)-dextran (150 kDa, Sigma-Aldrich, Saint Louis, MO, USA) as a macromolecule. FITC-dextran (0.5 mL) dissolved in saline (30 mg/mL) was injected via a tail vain of the t-MCAO rat model at 0, 1, 3, 6 or 24 h after reperfusion, respectively. One

hour after the injection, the brain was dissected and sliced into 2 mm thick coronal sections in the exactly same way as above experiment. All sections were put in grass slides and their fluorescence was measured at with in vivo imaging system (IVIS, Xenogen Corp., Alameda, CA).

REFERENCES

Back, T., 1998. Pathophysiology of the ischemic penumbra—revision of a concept. Cell. Mol. Neurobiol. 18, 621–638.

Cipolla, M.J., McCall, A.L., Lessov, N., Porter, J.M., 1997. Reperfusion decreases myogenic reactivity and alters middle cerebral artery function after focal cerebral ischemia in rats. Stroke 28, 176–180.

Cipolla, M.J., Curry, A.B., 2002. Middle cerebral artery function after stroke: the threshold duration of reperfusion for myogenic activity. Stroke 33, 2094–2099.

Cunningham, L.A., Wetzel, M., Rosenberg, G.A., 2005. Multiple roles for MMPs and TIMPs in cerebral ischemia. Glia 50, 329–339.

Dirnagl, U., Iadecola, C., Moskowitz, M.A., 1999. Pathobiology of ischaemic stroke: an integrated view. Trends Neurosci. 22, 391–397.

Erdo, F., Berzsenyi, P., Andrasi, F., 2005. The AMPA-antagonist talampanel is neuroprotective in rodent models of focal cerebral ischemia. Brain Res. Bull. 66, 43–49.

Huang, J., Upadhyay, U.M., Tamargo, R.J., 2006. Inflammation in stroke and focal cerebral ischemia. Surg. Neurol. 66, 232–245.

Kannan, S., Kolhe, P., Raykova, V., Glibatec, M., Kannan, R.M., Lieh-Lai, M., Bassett, D., 2004. Dynamics of cellular entry and drug delivery by dendritic polymers into human lung epithelial carcinoma cells. J. Biomater. Sci. Polym. Ed. 15, 311–330.

Kato, N., Yanaka, K., Hyodo, K., Homma, K., Nagase, S., Nose, T., 2003. Stable nitroxide Tempol ameliorates brain injury by inhibiting lipid peroxidation in a rat model of transient focal cerebral ischemia. Brain Res. 979, 188–193.

Kontos, H.A., 2001. Oxygen radicals in cerebral ischemia: the 2001 Willis lecture. Stroke 32, 2712–2716.

Lo, E.H., 2008. A new penumbra: transitioning from injury into repair after stroke. Nat. Med. 14, 497–500.

Lopez-Sanchez, C., Martin-Romero, F.J., Sun, F., Luis, L., Samhan-Arias, A.K., Garcia-Martinez, V., Gutierrez-Merino, C., 2007. Blood micromolar concentrations of kaempferol afford protection against ischemia/reperfusion-induced damage in rat brain. Brain Res. 1182, 123–137.

Lukyanov, A.N., Hartner, W.C., Torchilin, V.P., 2004. Increased accumulation of PEG-PE micelles in the area of experimental myocardial infarction in rabbits. J. Control. Release 94, 187–193.

Marler, J.R., Goldstein, L.B., 2003. Medicine. Stroke—tPA and the clinic. Science 301, 1677.

Nagasawa, H., Kogure, K., 1989. Correlation between cerebral blood flow and histologic changes in a new rat model of middle cerebral artery occlusion. Stroke 20, 1037–1043.

Rosenberg, G.A., Estrada, E.Y., Dencoff, J.E., 1998. Matrix metalloproteinases and TIMPs are associated with blood–brain barrier opening after reperfusion in rat brain. Stroke 29, 2189–2195.

Seymour, L.W., Miyamoto, Y., Maeda, H., Brereton, M., Strohalm, J., Ulbrich, K., Duncan, R., 1995. Influence of molecular weight on passive tumour accumulation of a soluble macromolecular drug carrier. Eur. J. Cancer. 31A, 766–770.

Svenson, S., 2009. Dendrimers as versatile platform in drug delivery applications. Eur. J. Pharm. Biopharm. 71, 445–462.

Xu, X.H., Zhang, S.M., Yan, W.M., Li, X.R., Zhang, H.Y., Zheng, X.X., 2006. Development of cerebral infarction, apoptotic cell death and expression of X-chromosome-linked inhibitor of apoptosis protein following focal cerebral ischemia in rats. Life Sci. 78, 704–712.

Yang, G.Y., Betz, A.L., 1994. Reperfusion-induced injury to the blood-brain barrier after middle cerebral artery occlusion in rats. Stroke 25, 1658–1664 discussion 1664-5.

Yang, Y., Estrada, E.Y., Thompson, J.F., Liu, W., Rosenberg, G.A., 2007. Matrix metalloproteinase-mediated disruption of tight junction proteins in cerebral vessels is reversed by synthetic matrix metalloproteinase inhibitor in focal ischemia in rat. J. Cereb. Blood Flow Metab. 27, 697–709.

Yoshida, H., Yanai, H., Namiki, Y., Fukatsu-Sasaki, K., Furutani, N., Tada, N., 2006. Neuroprotective effects of edaravone: a novel free radical scavenger in cerebrovascular injury. CNS Drug Rev. 12, 9–20.

Zhang, Z.G., Zhang, L., Tsang, W., Soltanian-Zadeh, H., Morris, D., Zhang, R., Goussev, A., Powers, C., Yeich, T., Chopp, M., 2002. Correlation of VEGF and angiopoietin expression with disruption of blood–brain barrier and angiogenesis after focal cerebral ischemia. J. Cereb. Blood Flow Metab. 22, 379–392.

Zhu, H.C., Gao, X.Q., Xing, Y., Sun, S.G., Li, H.G., Wang, Y.F., 2004. Inhibition of caspase-3 activation and apoptosis is involved in 3-nitropropionic acid-induced ischemic tolerance to transient focal cerebral ischemia in rats. J. Mol. Neurosci. 24, 299–305.

Journal of Controlled Release 141 (2010) 208–215

Contents lists available at ScienceDirect

Journal of Controlled Release

journal homepage: www.elsevier.com/locate/jconrel

Temperature-dependent transfer of amphotericin B from liposomal membrane of AmBisome to fungal cell membrane

Kosuke Shimizu [a], Masaaki Osada [a], Koji Takemoto [b], Yutaka Yamamoto [b], Tomohiro Asai [a], Naoto Oku [a,*]

[a] Department of Medical Biochemistry and Global COE program, School of Pharmaceutical Sciences, University of Shizuoka, 52-1 Yada, Suruga-ku, Shizuoka 422-8526, Japan
[b] Dainippon Sumitomo Pharma Co., Ltd., 1-98 Kasugade Naka 3-Chome, Konohana-ku, Osaka 554-0022, Japan

ARTICLE INFO

Article history:
Received 18 April 2009
Accepted 22 September 2009
Available online 6 October 2009

Keywords:
AmBisome
Temperature-dependency
Cell wall
Ergosterol
Membrane fluidity

ABSTRACT

Liposomal amphotericin B (AMPH-B), also known as AmBisome, exhibits a potent antifungal effect through its binding to ergosterol contained within the fungal cell membrane. However, the mechanism responsible for the movement of AmBisome-derived AMPH-B to the fungal cell membrane through the cell wall is not yet clear. Therefore, in the present study we aimed at elucidating this mechanism operating in *Saccharomyces cerevisiae*. AmBisome showed its antifungal effect against *S. cerevisiae* at 35 °C but not at 4 °C, whereas free AMPH-B was effective at both temperatures. A significant difference in the amount of AMPH-B transferred to the fungal cells between incubation at 4 and 35 °C was also observed when AmBisome was used. Confocal microscopic study, however, indicated that NBD-labeled AmBisome was localized on the surface of the fungal cells at either temperature. To decrease the affinity of AMPH-B for the liposomal membrane, we entrapped AMPH-B in fluid liposomes containing egg yolk phosphatidylcholine (EPC) instead of hydrogenated soy PC (HSPC). These liposomes showed the antifungal effect even at 4 °C. On the contrary, AMPH-B in liposomes containing ergosterol (Erg-AmB) instead of cholesterol showed a significantly weaker antifungal effect at 35 °C with reduced transfer of AMPH-B to the fungal cells. These results suggest that not the binding of AmBisome to target cells but the transfer of AMPH-B from liposomal membrane of AmBisome to the cell membrane is critical for the antifungal activity of AmBisome. This transfer is dependent on the temperature, fluidity of the liposomal membrane, and the affinity of AMPH-B for the fungal cell membrane.

1. Introduction

Since patients with infectious diseases caused by certain bacteria or fungi are at a high risk for death, the development of effective drugs for these diseases is of great importance. Mycosis is an infectious disease caused by fungal invasion, and it is divided into 3 classes based on the infection site. Among them, infection by fungi at deep internal organ such as lung and brain is the most serious and is known as deep mycosis. Amphotericin B (AMPH-B), a drug with strong antifungal activity, is effective against deep mycosis and also has a wide antibacterial spectrum [1,2]. As to its mechanism of action, AMPH-B is known to bind to ergosterol contained in the fungal cell membrane, which binding induces a permeability change in the membrane [3,4]. Since AMPH-B also has the ability to bind to cholesterol to some extent [5], it causes side effects such as nephrotoxicity [6]. In order to reduce the side effects of AMPH-B, a liposomal formulation of AMPH-B, known as AmBisome, has been developed. AmBisome is a small unilamellar vesicle containing AMPH-B that is stably retained in the hydrophobic part of the liposomal membrane by complexing with liposomal cholesterol. Since liposomalization of AMPH-B prolongs the circulation of AMPH-B in the bloodstream and decreases the transfer of AMPH-B to cell-membrane cholesterol, the use of AmBisome reduces the side effects of AMPH-B [7–11]. The mechanism of transfer of AMPH-B from AmBisome to the fungal membrane is still unclear, since AmBisome retains the drug in the liposomal membrane rather tightly. By electron microscopy Adler-Moore et al. previously examined the localization of liposomal lipids of AmBisome after exposure to fungal cells such as *Candida glabrata* and *Aspergillus fumigatus* and observed that AmBisome-derived lipids were distributed throughout the cytoplasm of the fungal cells after long-term incubation [12,13]. They also speculated that AmBisome has an affinity for the fungal cell wall and initially binds to it and that the liposomal lipids from AmBisome become dispersed throughout the cytoplasm after damage to the fungal cell membrane caused by AMPH-B released from disrupted AmBisome [13]. Their report indicates that the transfer of AmBisome-derived AMPH-B to the fungal cell membrane is a key step in the action of AmBisome against fungi.

In the present study, we aimed at elucidating the mechanism underlying the transfer of AMPH-B from AmBisome to the fungal cell membrane by using *Saccharomyces cerevisiae* as a model fungal cell. *S. cerevisiae* has a thick cell wall similar to that of other fungal cells [14].

Abbreviations: AMPH-B, amphotericin B; EPC, egg yolk phosphatidylcholine; EPG, egg yolk phosphatidylglycerol; DSPG, distearoylphosphatidylglycerol; HSPC, hydrogenated soy phosphatidylcholine; NBD-PE, *N*-4-nitrobenzo-2-oxa-13-diazol phosphatidylethanolamine.

* Corresponding author. Tel.: +81 54 264 5701; fax: +81 54 264 5705.
E-mail address: oku@u-shizuoka-ken.ac.jp (N. Oku).

0168-3659/$ – see front matter © 2009 Elsevier B.V. All rights reserved.
doi:10.1016/j.jconrel.2009.09.019

At first, we examined the temperature dependence of AmBisome activity against *S. cerevisiae*, and observed that, unlike AMPH-B, the antifungal activity of AmBisome was drastically suppressed at a low temperature. Then, we examined the localization of AmBisome in yeast cells at different temperatures by confocal laser-scanning microscopy and measured the amount of AMPH-B taken up into the cells. The transfer of AMPH-B from AmBisome to the cell and the antifungal activity of the liposomes were increased by raising the incubation temperature. Interestingly, AMPH-B in a fluid liposomal membrane was taken up into the cells more easily and was fungicidal at a low temperature. On the contrary, AMPH-B in ergosterol-containing liposomes was taken up into the cells in less amount; and the cytotoxic action was suppressed even at a high temperature. The results indicate the importance of translocation of AMPH-B from AmBisome to the cells in its antifungal activity.

2. Materials and methods

2.1. Reagents

AmBisome was the product of Dainippon Sumitomo Pharma Co., Ltd. (Osaka, Japan) Hydrogenated soy phosphatidylcholine (HSPC), distearoylphosphatidylglycerol (DSPG), egg yolk phosphatidylcholine (EPC), egg yolk phosphatidylglycerol (EPG), and cholesterol were gifts from Nippon Fine Chemical Co., Ltd. (Hyogo, Japan). Amphotericin B (AMPH-B), ergosterol, and *N*-4-nitrobenzo-2-oxa-13-diazol phosphatidylethanolamine (NBD-PE) were purchased from The United States Pharmacopeial Convention, Inc. (Rockville, MD, U.S.A.), Sigma-Aldrich Co. (St Louis, MO, U.S.A.), and Avanti Polar Lipids, Inc. (Alabaster, AL, U.S.A.), respectively. Rhodamine-dextran (10 kDa) was purchased from Wako Pure Chemical Industries, Ltd.

2.2. Yeast cell culture

Yeast cells of the *S. cerevisiae* ATCC 9763 (ATCC, U.S.A.) were used as a model of fungal cells in this experiment. They were colonized on YPD/agar medium and kept at 4 °C. Before experimental use, a single colony was picked up and grown in YPD medium with shaking at 30 °C for at least 12 h; and the OD_{600} of the cell suspension was adjusted to 0.1 using RPMI 1640 medium (Sigma-Aldrich Co.) buffered to pH 7.0 with 0.165 M MOPS (Dojindo Laboratories, Kumamoto, Japan).

2.3. Preparation of liposomes

AmBisome (liposomal AMPH-B) was composed of HSPC, DSPG, cholesterol, and AMPH-B (10:4:5:2 as a molar ratio). AmBisome solution was prepared by hydration of lyophilized AmBisomal components with ultrapure water. For preparation of NBD-labeled AmBisome, the lyophilized AmBisomal components were firstly dissolved in chloroform, after which NBD-PE solution was added to them. Then, they were lyophilized again with *t*-butanol and rehydrated with succinate-buffered solution (pH 5.5). Unincorporated NBD-PE was removed by gel filtration chromatography with a PD-10 column. For preparation of AmBisome encapsulating rhodamine-dextran, the lyophilized AmBisomal components were hydrated with rhodamine-dextran solution; and then free rhodamine-dextran was removed by column chromatography with Sepharose™ 4 Fast Flow (GE Healthcare UK Ltd., England). AMPH-B in liposomes containing ergosterol (Erg-AmB) was prepared with HSPC, DSPG, ergosterol, and AMPH-B (10:4:5:2 as a molar ratio). The thin lipid film containing AMPH-B was hydrated with succinate-buffered solution with 9% sucrose at 60 °C and freeze-thawed with liquid nitrogen for 3 cycles. The obtained liposomal solution was sized by sonication. Unincorporated AMPH-B was removed by column chromatography with Sepharose™ 4 Fast Flow. Liposomal AMPH-B composed of highly fluid phospholipids (Egg-AmB) was prepared with EPC, EPG, cholesterol, and AMPH-B (10:4:5:2 as a molar ratio) in the similar manner as used to prepare Erg-AmB. The particle size of each liposome was measured by dynamic light scattering analysis with a Zetasizer Nano (Malvern Instruments, Malvern, U.K.) and was about 100 nm in diameter.

2.4. Colony formation assay

Each liposomal AMPH-B diluted in succinate-buffered solution with 9% sucrose or free AMPH-B dissolved in 0.1% DMSO (final conc.) at a concentration of 20 μM as AMPH-B was added to a yeast cell suspension and incubated in MOPS-buffered RPMI 1640 medium at 4 or 35 °C for 0.5 or 3 h. Then, the cell suspension was centrifuged and washed twice with PBS. The cell pellet was resuspended in PBS and plated on YPD/agar medium. After 24 h of incubation at 30 °C, the number of colonies formed was counted.

2.5. Confocal microscopy

NBD-labeled liposomal AMPH-B (20 μM) was added to a yeast cell suspension, which was then incubated in MOPS-buffered RPMI 1640 medium at 4 or 35 °C for 3 or 24 h with shaking. After having been washed 3 times with PBS, the cells were fixed with 4% paraformaldehyde and stained with Fluorescent Brightener 28 (Sigma-Aldrich Co., U.S.A.) for cell-wall imaging. After another 3 washes with PBS, the cells were attached to MAS-coated glass slides (Matsunami Glass Ind., Ltd., Japan) by centrifugation, and then localization of liposomes in yeast cells was observed under an LSM510 META confocal laser-scanning microscope (Carl Zeiss, Inc., Germany).

2.6. Measurement of the amount of AMPH-B transferred to yeast cells

Liposomal AMPH-B (20 μM) was added to a yeast cell suspension, which was then incubated in MOPS-buffered RPMI 1640 medium with shaking at 4 or 35 °C for 0.5 or 3 h. After having been washed with PBS, the cells were disrupted by using glass beads with shaking and sonication, and AMPH-B in the cells was extracted with methanol. After centrifugation, the methanol extract was evaporated; and the residual AMPH-B was dissolved in the mobile phase for HPLC analysis. The HPLC conditions were the following: Column, TSKgel ODS-100Z 4.6×250 mm (Tosoh Co., Japan); mobile phase, acetonitrile and 2.5 mM EDTA (pH 5.0), 4:6 (v/v); temperature, 35 °C; injection volume, 50 μL; flow rate, 1.0 mL/min; and UV detection, 405 nm. Smart Chrom software was used for control of the HPLC system and data processing.

In the inhibition experiment, AmBisome was added to a yeast cell suspension, which was subsequently incubated in the presence or absence of drug free cholesterol liposomes (Cho-Lip) or vacant ergosterol liposomes (Erg-Lip) in MOPS-buffered RPMI 1640 medium. After a 3-h incubation, the amount of AMPH-B transferred to the cells was measured.

2.7. Investigation of AmBisome disruption

Rhodamine-encapsulating AmBisome was added to different numbers of yeast cells ($OD_{600}=0.1$ or 0.3), and the cells were incubated in MOPS-buffered RPMI 1640 medium for 0.5 or 3 h at 4 or 35 °C. After centrifugation for washing, the supernatant medium was collected and ultracentrifuged to separate the intact AmBisome into the pellet. The resulting supernatant was then collected, and the fluorescence intensity of the rhodamine-dextran that had been released into the medium from AmBisome was measured.

2.8. FRAP experiment

NBD-labeled AmBisome and Egg-AmB were similarly prepared as described above and then gradually frozen to make giant-sized liposomes. Then, these liposomes were applied on MAS-coated slide glasses and dried in the dark at room temperature for overnight. FRAP experiments were performed with LSM510 META confocal laser-

scanning microscope according to the protocol of LSM510 for FRAP experiment.

2.9. Statistic analysis

The variance in a group was evaluated by use of the *F*-test, and the differences among the groups were evaluated by using Student's *t*-test.

3. Results

3.1. Temperature-dependent antifungal activity of AmBisome against S. cerevisiae

To confirm the temperature dependence of AmBisome antifungal activity, we evaluated the effect of AmBisome against *S. cerevisiae* at 4 or 35 °C by using the colony formation assay. As shown Fig. 1A, AmBisome showed time-dependent antifungal activity against yeast cells at 35 °C. Free AMPH-B showed stronger antifungal activity than AmBisome, and no colonies were found even after just 0.5 h of incubation with it at 35 °C. On the other hand, the antifungal effect of AmBisome was significantly reduced at 4 °C incubation (Fig. 1B), and the number of colonies was quite similar to that of the control, suggesting the antifungal effect of AmBisome to be temperature-dependent. In contrast, free AMPH-B showed strong fungicidal activity even at this temperature. These results are summarized in Fig. 1C.

3.2. Binding of AmBisome to the surface of yeast cells

In general, intact liposome is unable to pass through the fungal cell wall due to its particle size. However, the cell wall penetration of AmBisome has not been fully elucidated, and it is not clear when or where AmBisome-derived AMPH-B is transferred to the fungal cell membrane. To elucidate the mechanism, we prepared NBD-labeled AmBisome and used confocal laser-scanning microscopy to observe its localization in yeast cells after exposure. AmBisome was observed to bind to the surface of yeast cells after a 3-h exposure at 35 °C (Fig. 2A). Especially, AmBisome often bound to budding or interface site of yeast cells. Furthermore, AmBisome-derived fluorescence was observed in the cytoplasm after 24 h of incubation at this temperature (Fig. 2B). Although liposomes without encapsulated AMPH-B also bound to the cell surface, they were not incorporated into the cytoplasm after a 24-h incubation (data not shown). On the other hand, similar to the 35 °C incubation, AmBisome bound to the cell surface after a 3-h incubation at 4 °C (Fig. 2A). However, unlike that at 35 °C, AmBisome-derived fluorescence was present only on the cell surface after 24 h of incubation at the lower temperature (Fig. 2B). The cellular uptake of AmBisome after 24 h incubation at 35 °C, would be the result of permeability increase in cell membrane caused by AMPH-B transferred to the membrane, since the distribution of NBD-labeled AmBisome in *S. cerevisiae* in the presence of free AMPH-B at 4 °C, NBD-labeled AmBisome was observed in the cytosol (data not shown).

3.3. Temperature-dependent transfer of AMPH-B from AmBisome to yeast cells

Next, we compared the amount of AMPH-B transferred to yeast cells at different incubation temperatures. AmBisome was added to the yeast cell suspension, and the cells were incubated at 4 or 35 °C. Thereafter, the amount of AMPH-B transferred to the cells was determined by HPLC. As a result, the amount of AMPH-B in the yeast cells was reduced at 4 °C of incubation (Fig. 3), suggesting that this transfer mechanism of AMPH-B from AmBisome is temperature-dependent.

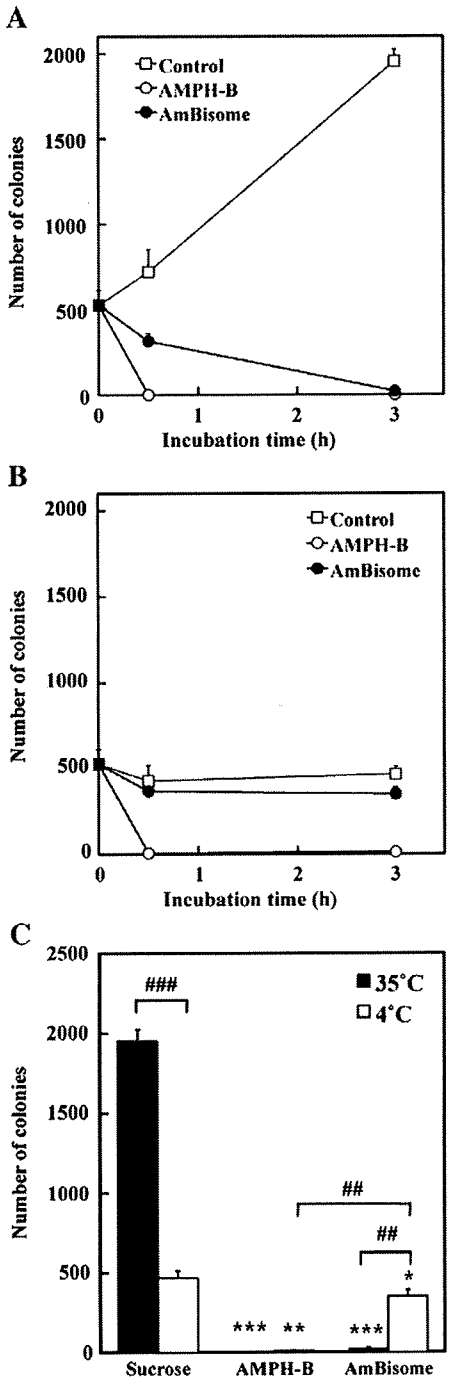

Fig. 1. Temperature-dependent antifungal activity of AmBisome against *Saccharomyces cerevisiae*. After the optical density of a *S. cerevisiae* suspension was adjusted to 0.1, sucrose, AMPH-B, or AmBisome (20 μM as AMPH-B) was added to the yeast cell suspension; and incubation was carried out at 35 °C (A) or 4 °C (B) for 0.5 or 3 h in MOPS-buffered RPMI 1640 medium. After the cells had been washed with PBS, they were plated on YPD/agar medium. After 24 h of incubation at 30 °C, the number of colonies formed was counted. The difference in activity between temperatures is also summarized (C). Significant differences are shown (* $P<0.05$, ** $P<0.01$, *** $P<0.001$ *vs.* Sucrose; ## $P<0.01$, ### $P<0.001$ as indicated by the brackets).

3.4. Disruption of AmBisome at the yeast cell surface

It is not clear whether or not the disruption of AmBisome is a prerequisite for AMPH-B release from the liposomal membrane after

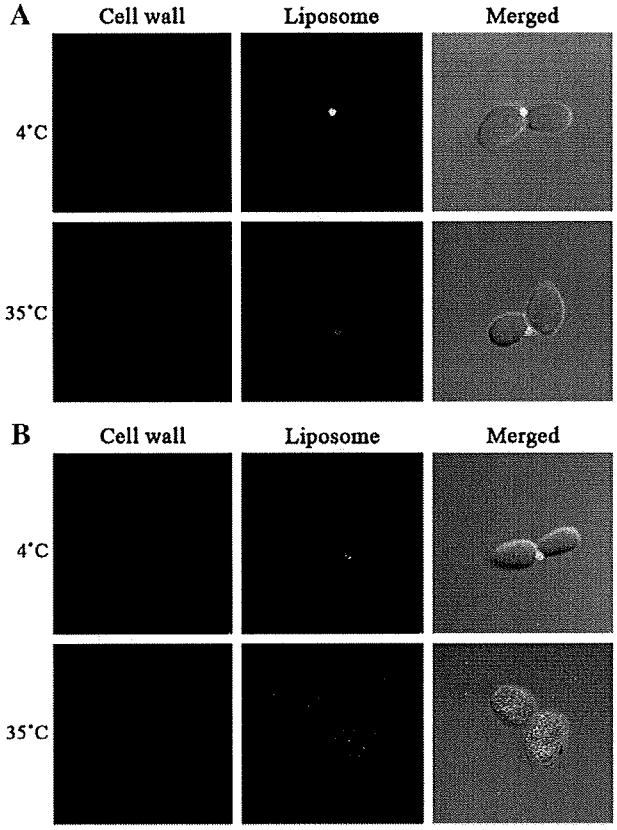

Fig. 2. Binding of AmBisome to cell wall of yeast cells. NBD-labeled AmBisome was added to yeast cell suspensions that were then incubated in MOPS-buffered RPMI 1640 medium at 4 or 35 °C for 3 h (A) or 24 h (B). Then, the yeast cell wall was stained with Fluorescent Brightener 28, and localization of AmBisome was observed with a confocal laser-scanning microscope. Green and blue images show AmBisome and the cell wall, respectively. Bar indicates 10 μm.

binding of AmBisome to the surface of yeast cells. To clarify this point, we prepared rhodamine-encapsulated AmBisome and investigated the disruption of the liposomes after exposure of the yeast cells to it.

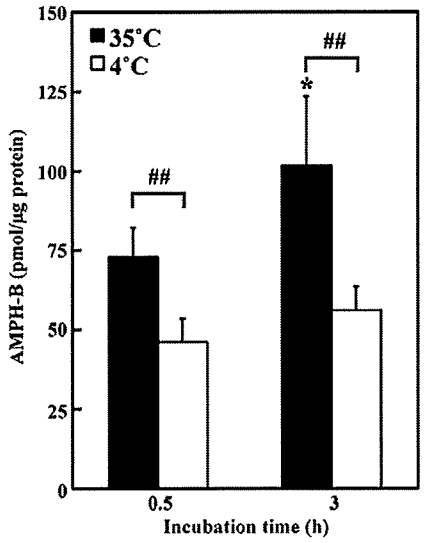

Fig. 3. Temperature-dependent transfer of AMPH-B to yeast cells. AmBisome was added to cell suspensions of *Saccharomyces cerevisiae* that were then incubated in MOPS-buffered RPMI 1640 medium at 4 or 35 °C for 0.5 or 3 h. After the cells had been washed with PBS, the amount of AMPH-B in the yeast cells was measured by HPLC. Significant differences are indicated (* $P<0.05$ *vs.* 35 °C; ## $P<0.01$, as indicated by the brackets).

When rhodamine-encapsulated AmBisome was incubated with yeast cells at a low density or number at 35 °C, the fluorescence of rhodamine released from AmBisome was very little, and most of the fluorescence was detected in the liposome fraction (Fig. 4A). A similar result was obtained even when the number of yeast cells was increased. Furthermore, there was no apparent difference in liposomal disruption between at 4 and 35 °C incubation (Fig. 4B). These results suggest that AmBisome was not disrupted at least until 3 h after binding to the cell surface and that AmBisome-derived AMPH-B was transferred to the fungal cell membrane without liposomal disruption.

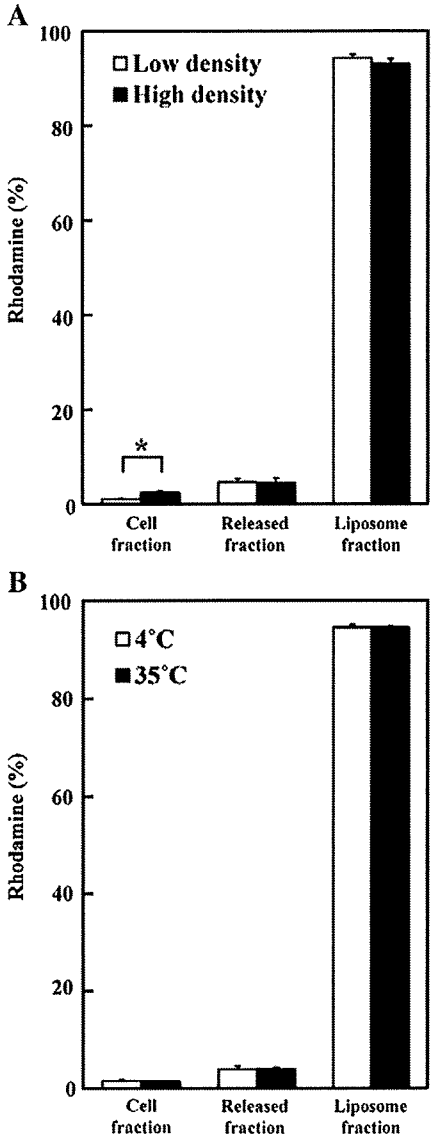

Fig. 4. Investigation of liposomal disruption during exposure of yeast cells to AmBisome. Rhodamine-encapsulating AmBisome was added to a suspension of *Saccharomyces cerevisiae* that had been adjusted to a low ($OD_{600}=0.1$) or high ($OD_{600}=0.3$) density, and the cells were then incubated in MOPS-buffered RPMI 1640 medium at 35 °C for 3 h (A). The culture medium was collected and ultracentrifuged to remove intact AmBisome. The fluorescence intensity of the rhodamine that had been released from rhodamine-encapsulating AmBisome into the medium was measured in the supernatant. Disruption of AmBisome at 4 °C was also examined (B). Asterisk shows a significant difference between bracketed values (* $P<0.05$).

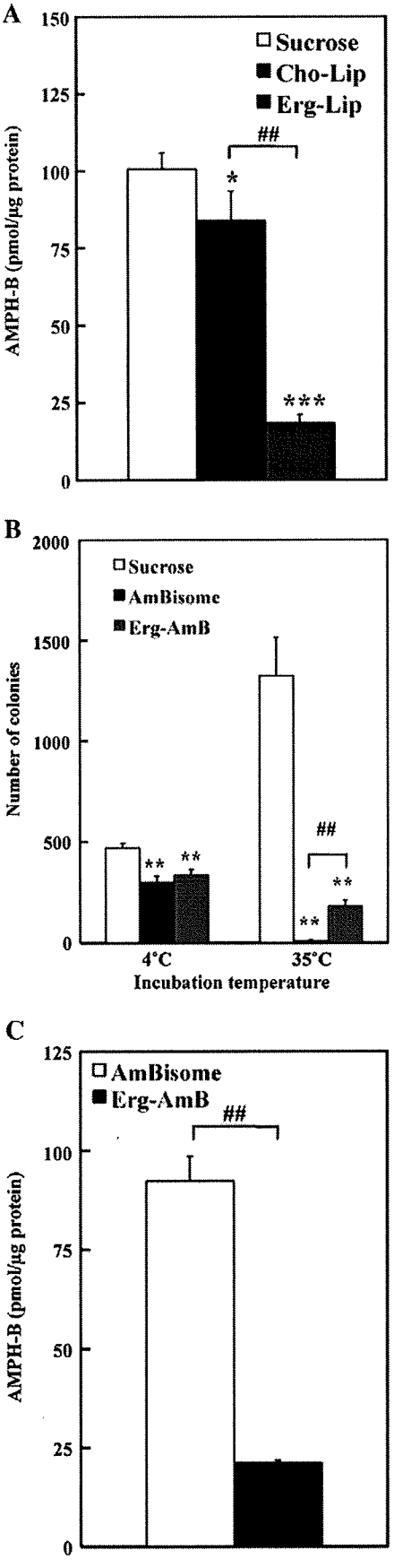

3.5. Importance of differential AMPH-B affinity for AmBisome and yeast cell membrane

To examine the importance of AMPH-B affinity for the fungal cell membrane during the transfer of AmBisome-derived AMPH-B to the membrane, we examined the transfer of AMPH-B to yeast cells in the presence of cholesterol liposomes (Cho-Lip) or ergosterol liposomes (Erg-Lip) in which AMPH-B was not entrapped. As a result, the transfer of AMPH-B from AmBisome was significantly reduced in the presence of Erg-Lip, whereas little inhibition was observed in the presence of Cho-Lip (Fig. 5A), confirming that the affinity of AMPH-B for ergosterol-containing membrane is stronger than that for cholesterol-containing one.

Next, we prepared liposomal AMPH-B containing ergosterol (Erg-AmB) instead of cholesterol and examined the antifungal activity of Erg-AmB against yeast cells. At 4 °C, the antifungal activity of Erg-AmB was attenuated just as in the case of AmBisome (Fig. 5B). However, at 35 °C Erg-AmB failed to kill all of the yeast cells whereas AmBisome completely destroyed them at this temperature (Fig. 5B). Furthermore, when the transfer of AMPH-B from Erg-AmB to the cells was investigated, the amount of AMPH-B in the cells was reduced after 3 h of incubation (Fig. 5C). These results indicate that ergosterol in the liposomes controlled the antifungal effect of liposomal AMPH-B and that the different affinity of AMPH-B for cholesterol and ergosterol played an important role in the transfer of AMPH-B to the fungal cell membrane.

3.6. Importance of liposomal membrane fluidity in temperature-dependent antifungal activity of AmBisome

Since the transfer of AMPH-B from AmBisome to the fungal cell membrane was dependent on the incubation temperature, we hypothesized that liposome membrane fluidity was a key factor in the transfer of AMPH-B. To examine the importance of membrane fluidity on the transfer of AMPH-B from AmBisome, we prepared AMPH-B liposomes composed of the highly fluid phospholipids EPC and EPG (Egg-AmB) instead of HSPC and DPPG. To measure the membrane fluidity of both liposomes, fluorescence recovery after photobleaching (FRAP) experiment was performed. NBD-labeled both liposomes were prepared, and FRAP measurement was recorded by using confocal laser scanning microscope (LSM510META). As a result, the fluorescence of NBD-PE in NBD-labeled Egg-AmB was recovered to more than 80% at 50 s after photobleaching and the diffusion coefficient was $8.2 \times 10^{-2} \mu m^2/s$, whereas the recovery of fluorescence in NBD-labeled AmBisome was little observed. This result indicates that liposome membrane fluidity of Egg-AmB is far higher than that of AmBisome. Then, the antifungal effect of Egg-AmB against *S. cerevisiae* was investigated at 4 or 35 °C incubation. Egg-AmB not only completely damaged yeast cells at 35 °C, but also showed the antifungal effect at 4 °C to some extent (Fig. 6A). When localization of NBD-labeled Egg-AmB in the yeast cells was observed under the confocal laser-scanning microscope, the fluorescence of Egg-AmB was present in the cytoplasm at both 4 and 35 °C after a 3-h incubation (Fig. 6B), whereas similar images were observed only after a 24-h incubation with AmBisome at 35 °C (Fig. 2B). Furthermore, the increase in the amount

Fig. 5. Effect of ergosterol on antifungal activity of AmBisome. AmBisome was added to yeast cell suspensions of *Saccharomyces cerevisiae* that were then incubated in the absence or presence of drug-free cholesterol liposome (Cho-Lip) or drug-free ergosterol liposome (Erg-Lip) for 3 h at 35 °C in MOPS-buffered RPMI 1640 medium. Then, the amount of AMPH-B in the cells was measured (A). Yeast cells were also incubated with sucrose, AmBisome or liposomal AMPH-B containing ergosterol (Erg-AmB) at 4 or 35 °C for 3 h. After the cells had been washed with PBS, they were plated on YPD/agar medium. After a 24-h incubation at 30 °C, the number of formed colonies was counted (B). The amount of AMPH-B in yeast cells after 3 h of incubation at 35 °C was also measured (C). Significant differences are shown (* $P<0.05$, ** $P<0.01$, *** $P<0.001$ *vs.* Sucrose; ## $P<0.01$, as indicated by the bracket).

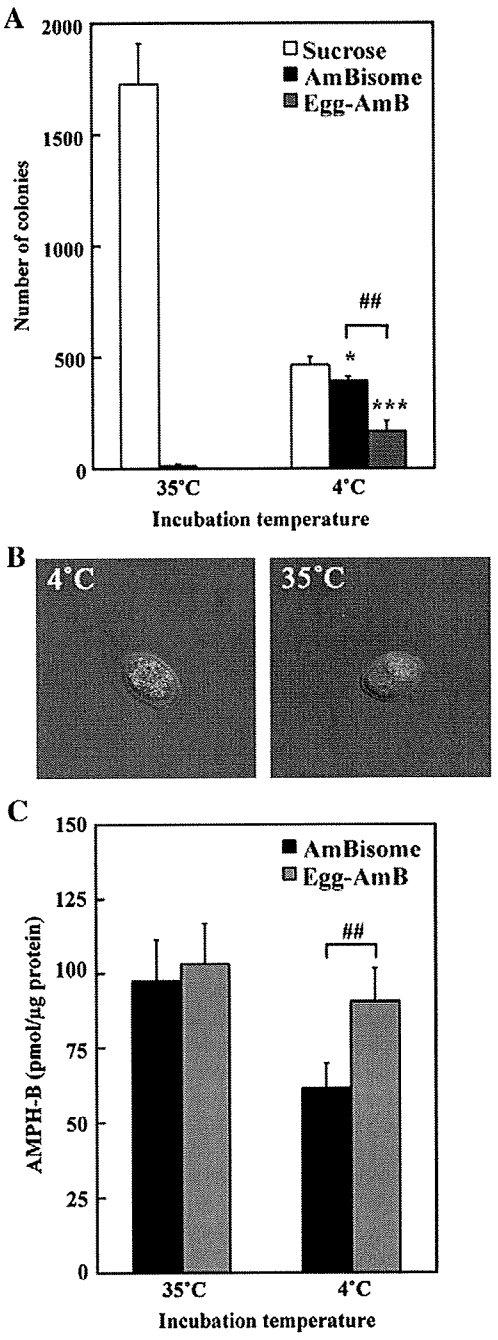

Fig. 6. Effect of liposome-membrane fluidity on antifungal activity of AmBisome. Cell suspensions of *Saccharomyces cerevisiae* were incubated with sucrose, AmBisome or liposomal AMPH-B composed of EPC and EPG (Egg-AmB) at 4 or 35 °C for 3 h in MOPS-buffered RPMI 1640 medium. After the cells had been washed with PBS, they were plated on YPD/agar medium. After 24 h of incubation at 30 °C, the number of colonies formed was counted (A). Localization of NBD-labeled Egg-AmB after a 3-h incubation at 4 or 35 °C was observed (B) and the amount of AMPH-B in the yeast cells after 3 h of incubation at 4 or 35 °C was also measured (C). Significant differences are shown (* $P<0.05$, *** $P<0.001$ vs. Sucrose; ## $P<0.01$, as indicated by the bracket).

of AMPH-B transferred from Egg-AmB to the cells after the 4 °C incubation was obvious (Fig. 6C). These results suggest that liposomal membrane fluidity was involved in the transfer of AMPH-B from AmBisome to the fungal cell membrane and indicate that AMPH-B in fluid liposomes would be easier to transfer to other membranes with high affinity for AMPH-B.

4. Discussion

It is known that liposomalization or polymerization of a drug often enables enhancement of the therapeutic effects and reduces the side effects by improving the pharmacokinetics and pharmacodynamics of the original drug in the body [15,16]. The liposomal antifungal drug AmBisome is a representative example of a liposome that incorporates AMPH-B in its membrane, enhances the stability of AMPH-B in the bloodstream and reduces the side effects of the drug [9,10]. AmBisome shows a potent antifungal effect against fungal cells such as *Candida albicans*, *Cryptococcus neoformans*, and *Aspergillus fumigatus*, resulting in the successful treatment of deep mycosis caused by them [17,18]. AmBisome exerts its effect by the binding of AMPH-B from AmBisome to ergosterol in the fungal cell membrane, which binding enhances the permeability of the fungal cell membrane and promotes the leakage of cellular substances and subsequent fungal cell death [3,19]. Thus, the transfer of AMPH-B from AmBisome to the fungal cell membrane is a key step for AmBisome to manifest its antifungal activity. In the case of other liposomal drugs, the release of the encapsulated drug from the liposome is critical for drug activity. For example, liposomal doxorubicin shows a potent cytotoxic effect against various kinds of cancer. The action mechanism of liposomal doxorubicin is considered to be as follows: Liposomal doxorubicin is incorporated into the cells by the endocytic pathway, the liposome is disrupted in lysosomes, and the encapsulated doxorubicin is released and transferred to nuclei to damage the cell. On the other hand, it is expected that the action mechanism of AmBisome against fungal cells would be different from that of other liposomal drugs against mammalian cells, since fungal cells possess a protective cell wall around their cell membrane, unlike mammalian cells [20]. In fact, it has not been fully clarified whether AmBisome can pass through the cell wall or not. In the present study, we aimed at elucidating the action mechanism of AmBisome, especially the mechanism of the transfer of AMPH-B from the liposome to ergosterol in the fungal cell membrane.

We firstly focused on the temperature dependence of AmBisome activity by comparing the antifungal effect of AmBisome against *S. cerevisiae* at 4 and 35 °C. As a result, AmBisome showed strong time-dependent antifungal activity at 35 °C, whereas free AMPH-B eradicated the yeast cells completely after just a 0.5-h incubation (Fig. 1A), indicating that AmBisome required a certain period of time to show its antifungal activity compared with AMPH-B. Furthermore, AmBisome did not show the activity at 4 °C, whereas AMPH-B showed strong activity at this same temperature (Fig. 1B, C). These results suggest that antifungal activity of AmBisome is dependent on the release and transfer of its AMPH-B to the fungal cell membrane. This temperature-dependent AmBisome activity would not be due to a difference in the localization of AmBisome in yeast cells, since AmBisome bound to yeast cells similarly at both 4 and 35 °C (Fig. 2A). Similar binding of AmBisome at 4 and 35 °C was also observed after a 0.5-h incubation (data not shown). These data also support the idea that the release and transfer of AMPH-B from AmBisome is critical for the antifungal efficacy instead of a temperature-dependent amount of AmBisome binding. In fact, the amount of AMPH-B transferred from AmBisome increased in a temperature-dependent manner (Fig. 3).

Adler-Moore et al. previously reported that gold-labeled AmBisome binds to the fungal cell wall, as observed by electron microscopy [13]. In our study, AmBisome actually bound to the cell wall and was topically observed to become localized at the budding or interface site of *S. cerevisiae* after a 3-h incubation at either 4 or 35 °C (Fig. 2A). In their review article Lesage et al. stated that the structure and components of the yeast cell wall change according to cell growth and are especially different during bud emergence and at the mother/daughter interface [21]. Thus, we hypothesize that these regions of the cell wall are susceptible to binding by AmBisome and that its

AMPH-B is transferred to the fungal cell membrane at these regions in a temperature-dependent manner. However, further research will be needed to elucidate whether AmBisome directly interacts with the fungal cell membrane or not.

Furthermore, AmBisome-derived fluorescence was present in the cytoplasm after 24 h of incubation at 35 °C but not at 4 °C (Fig. 2B). We speculate that the fungal cell death causes the entry of AmBisome into the cytoplasm.

We next examined the possible disruption of AmBisome for the transfer of AMPH-B to the fungal cell membrane. As a result, AmBisome-derived rhodamine release was minimal after exposure to the drug, even when the number of yeast cells was increased or the incubation temperature was changed (Fig. 4). These results indicate that the transfer of AMPH-B from AmBisome occurred at least until 3 h after attachment to the outside of fungal cells without disruption of the liposomal architecture of AmBisome.

Finally, to identify the key factor for the transfer of AMPH-B from AmBisome, we prepared liposomal AMPH-B with different lipid compositions and investigated the effect of lipid composition on AmBisome-induced antifungal activity. When AMPH-B was incorporated into liposomes containing ergosterol instead of cholesterol, the antifungal effect against *S. cerevisiae* was significantly reduced compared with that of AmBisome at 35 °C, where the membrane fluidity is considered to be similar (Fig. 5B). In addition, the amount of transferred AMPH-B to the yeast cells from Erg-AmB was decreased (Fig. 5C). It is known that the affinity of AMPH-B for ergosterol is about 10 times higher than that for cholesterol [22]. Thus, this result suggests that liposomal ergosterol prevented the release of AMPH-B from liposomes, the consequence being suppression of the transfer of AMPH-B from AmBisome to the fungal cell surface. A number of studies have been presented about the reason for the high affinity of AMPH-B to ergosterol in comparison with that to choresterol. Recently, Baran et al. suggested that AmB-ergosterol-AmB aggregates simulated of 2:1 stoichiometry retain significantly higher stability and relatively rigid, "sandwich" geometry due to Van der Waals forces and the intermolecular hydrogen bonds [23]. In contrast, cholesterol does not form this sandwich geometry that would be the reason for the low affinity of AMPH-B to cholesterol in comparison with this to ergosterol [23].

On the contrary, when AMPH-B was incorporated into liposomes composed of high-fluidity phospholipids, namely, EPC and EPG, the antifungal effect against *S. cerevisiae* was observed even at 4 °C, where the membrane fluidity is rather low and AmBisome showed little effect (Fig. 6A). In addition, the amount of AMPH-B transferred to the yeast cells from Egg-AmB was increased (Fig. 6C). When localization of NBD-labeled Egg-AmB in the yeast cells was examined, the fluorescence of Egg-AmB was present in the cytoplasm even after 0.5 h of incubation (Fig. 6B). It is known that the phase-transition temperature of EPC and HSPC is about −10 °C and 55 °C, respectively. When the membrane fluidity of Egg-AmB and AmBisome was compared using NBD-PE by FRAP experiment, the membrane fluidity of Egg-AmB is higher than that of AmBisome. According to the result, it is reasonable that the transfer of AMPH-B from Egg-AmB to the fungal cell membrane would occur at the low temperature. Thus, these results suggest that the increased membrane fluidity enhanced the release of AMPH-B from AmBisome and stability of AMPH-B in the liposomal membrane is the key factor for the biological activity of liposomal AMPH-B.

According to the report by Legrand et al., the critical micelle concentration (CMC) of AMPH-B was 0.1 μM in aqueous solution. They showed that the concentration of free AMPH-B released by AmBisome at 1 μg/ml (1.08 μM) was about 0.08 μg/ml (0.09 μM), which was below the CMC of AMPH-B [24]. We investigated the release of AMPH-B from AmBisome at high concentration (2.22 mM) in MOPS-buffered RPMI 1640 medium at room temperature using an ultrafiltration method. As a result, time-dependent release of AMPH-B was not observed (0.293 and 0.369 μM at 0 and 24 h after incubation, respectively; 0.013% and 0.017% of total AMPH-B in AmBisome), suggesting that AmBisome is quite stable, but allows the release of a little amount of AMPH-B (data not shown). Based on such information and results obtained in the present study, we hypothesized that ergosterol in the fungal cell membrane may be able to increase the amount of AMPH-B released from AmBisome or induce the continuous release of AMPH-B from AmBisome without direct interaction to AmBisome after AmBisome attachment to the fungal cell wall.

5. Conclusion

Our present study demonstrated that AmBisome bound to the cell wall of yeast cells and that the AMPH-B from AmBisome was transferred to the yeast cell membrane without obvious disruption of the liposome formulation. Furthermore, we demonstrated that the transfer of AMPH-B was dependent on temperature and fluidity of the liposome membrane.

Acknowledgements

The authors thank all members of the Department of Medical Biochemistry at the University of Shizuoka for their helpful advice in this study.

Appendix A. Supplementary data

Supplementary data associated with this article can be found, in the online version, at doi:10.1016/j.jconrel.2009.09.019.

References

[1] M.E. Klepser, E.J. Wolfe, R.N. Jones, C.H. Nightingale, M.A. Pfaller, Antifungal pharmacodynamic characteristics of fluconazole and amphotericin B tested against *Candida albicans*, Antimicrob. Agents Chemother. 41 (6) (1997) 1392–1395.
[2] L. Ostrosky-Zeichner, K.A. Marr, J.H. Rex, S.H. Cohen, Amphotericin B: time for a new "gold standard", Clin. Infect. Dis. 37 (3) (2003) 415–425.
[3] B.E. Cohen, Concentration- and time-dependence of amphotericin-B induced permeability changes across ergosterol-containing liposomes, Biochim. Biophys. Acta 857 (1) (1986) 117–122.
[4] I. Fournier, J. Barwicz, P. Tancrede, The structuring effects of amphotericin B on pure and ergosterol- or cholesterol-containing dipalmitoylphosphatidylcholine bilayers: a differential scanning calorimetry study, Biochim. Biophys. Acta 1373 (1) (1998) 76–86.
[5] K.M. Wasan, G. Lopez-Berestein, The interaction of liposomal amphotericin B and serum lipoproteins within the biological milieu, J. Drug Target 2 (5) (1994) 373–380.
[6] R. Sabra, R.A. Branch, Amphotericin B nephrotoxicity, Drug Saf 5 (2) (1990) 94–108.
[7] I. Bekersky, R.M. Fielding, D.E. Dressler, J.W. Lee, D.N. Buell, T.J. Walsh, Plasma protein binding of amphotericin B and pharmacokinetics of bound versus unbound amphotericin B after administration of intravenous liposomal amphotericin B (AmBisome) and amphotericin B deoxycholate, Antimicrob. Agents Chemother. 46 (3) (2002) 834–840.
[8] J. Adler-Moore, R.T. Proffitt, Effect of tissue penetration on AmBisome efficacy, Curr. Opin. Investig. Drugs 4 (2) (2003) 179–185.
[9] K. Takemoto, Y. Yamamoto, Y. Ueda, Evaluation of antifungal pharmacodynamic characteristics of AmBisome against *Candida albicans*, Microbiol. Immunol. 50 (8) (2006) 579–586.
[10] K. Takemoto, Y. Yamamoto, Y. Ueda, Y. Sumita, K. Yoshida, Y. Niki, Comparative study on the efficacy of AmBisome and Fungizone in a mouse model of pulmonary aspergillosis, J. Antimicrob. Chemother. 57 (4) (2006) 724–731.
[11] E. Briones, C.I. Colino, J.M. Lanao, Delivery systems to increase the selectivity of antibiotics in phagocytic cells, J. Control Release 125 (3) (2008) 210–227.
[12] J. Adler-Moore, AmBisome targeting to fungal infections, Bone Marrow Transplant. 14 (Suppl 5) (1994) S3–7.
[13] J. Adler-Moore, R.T. Proffitt, AmBisome: liposomal formulation, structure, mechanism of action and pre-clinical experience, J. Antimicrob. Chemother 49 (Suppl 1) (2002) 21–30.
[14] V.J. Cid, A. Duran, F. del Rey, M.P. Snyder, C. Nombela, M. Sanchez, Molecular basis of cell integrity and morphogenesis in *Saccharomyces cerevisiae*, Microbiol. Rev. 59 (3) (1995) 345–386.
[15] T.M. Allen, P.R. Cullis, Drug delivery systems: entering the mainstream, Science 303 (5665) (2004) 1818–1822.
[16] G. Gaucher, M.H. Dufresne, V.P. Sant, N. Kang, D. Maysinger, J.C. Leroux, Block copolymer micelles: preparation, characterization and application in drug delivery, J. Control Release 109 (1–3) (2005) 169–188.

[17] J.P. Adler-Moore, S.M. Chiang, A. Satorius, D. Guerra, B. McAndrews, E.J. McManus, R.T. Proffitt, Treatment of murine candidosis and cryptococcosis with a unilamellar liposomal amphotericin B formulation (AmBisome), J. Antimicrob. Chemother 28 (Suppl B) (1991) 63–71.
[18] A.C. Leenders, P. Reiss, P. Portegies, K. Clezy, W.C. Hop, J. Hoy, J.C. Borleffs, T. Allworth, R.H. Kauffmann, P. Jones, F.P. Kroon, H.A. Verbrugh, S. de Marie, Liposomal amphotericin B (AmBisome) compared with amphotericin B both followed by oral fluconazole in the treatment of AIDS-associated cryptococcal meningitis, AIDS 11 (12) (1997) 1463–1471.
[19] M. Baginski, H. Resat, E. Borowski, Comparative molecular dynamics simulations of amphotericin B-cholesterol/ergosterol membrane channels, Biochim. Biophys. Acta 1567 (1–2) (2002) 63–78.
[20] M. Kirkham, R.G. Parton, Clathrin-independent endocytosis: new insights into caveolae and non-caveolar lipid raft carriers, Biochim. Biophys. Acta 1745 (3) (2005) 273–286.
[21] G. Lesage, H. Bussey, Cell wall assembly in *Saccharomyces cerevisiae*, Microbiol. Mol. Biol. Rev. 70 (2) (2006) 317–343.
[22] J.D. Readio, R. Bittman, Equilibrium binding of amphotericin B and its methyl ester and borate complex to sterols, Biochim. Biophys. Acta 685 (2) (1982) 219–224.
[23] M. Baran, E. Borowski, J. Mazerski, Molecular modeling of amphotericin B-ergosterol primary complex in water II, Biophys. Chem. 141 (2–3) (2009) 162–168.
[24] P. Legrand, M. Cheron, L. Leroy, J. Bolard, Release of amphotericin B from delivery systems and its action against fungal and mammalian cells, J. Drug Target 4 (5) (1997) 311–319.

Cancer Letters 287 (2010) 165–171

Contents lists available at ScienceDirect

Cancer Letters

journal homepage: www.elsevier.com/locate/canlet

A novel DDS strategy, "dual-targeting", and its application for antineovascular therapy

Yuki Murase [a], Tomohiro Asai [a], Yasufumi Katanasaka [a], Tomoki Sugiyama [a], Kosuke Shimizu [a], Noriyuki Maeda [b], Naoto Oku [a,*]

[a] Department of Medical Biochemistry and Global COE Program, Graduate School of Pharmaceutical Sciences, University of Shizuoka, 52-1 Yada, Suruga-ku, Shizuoka 422-8526, Japan
[b] Nippon Fine Chemical Co. Ltd., Takasago, Hyogo 676-0074, Japan

ARTICLE INFO

Article history:
Received 16 December 2008
Received in revised form 25 March 2009
Accepted 8 June 2009

Keywords:
Dual-targeting
Drug delivery system
Liposomes
Active-targeting
Antineovascular therapy
Angiogenesis

ABSTRACT

Dual-targeting liposomes modified with Ala-Pro-Arg-Pro-Gly (APRPG) and Gly-Asn-Gly-Arg-Gly (GNGRG) peptides were developed. They remarkably associated to growing human umbilical vein endothelial cells (HUVECs) compared with single-targeting liposomes modified with APRPG or GNGRG. Doxorubicin (DOX) encapsulated in the dual-targeting liposomes significantly suppressed the growth of HUVECs compared with that in single-targeting liposomes. The dual-targeting liposomes containing DOX strongly suppressed tumor growth in Colon26 NL-17 carcinoma-bearing mice. Confocal microscopic data indicated that this anticancer effect was brought by the association of these liposomes to angiogenic vessels in the tumor. These findings suggest that "dual-targeting" would be a hopeful method for targeting therapies.

1. Introduction

Liposomes are known as one of the most effective drug carriers for cancer therapy. In liposomal DDS technologies, polyethylene glycol (PEG)-modified liposomes are well known as useful drug carriers for cancer therapy. PEG-modified liposomes have long-circulating characteristics through avoidance of trapping by a reticuloendothelial system (RES) such as liver and spleen [1,2]. PEG-modified liposomes tend to accumulate in tumor tissues thorough passive targeting since leaky angiogenic vessels brings enhanced permeability and retention (EPR) effect [3,4]. In fact, PEG-modified liposomes containing doxorubicin (DOX) have been used in clinical cancer therapy. On the other hand, active-targeting using liposomes modified with ligands such as antibodies and peptides achieves more selective drug delivery to tumor tissues. These ligands that recognize tumor-associated molecules are conjugated to the head of PEG-chain of liposomes [5,6]. Active-targeting using ligand-modified long-circulating PEG-liposomes would be more effective since these liposomes have great opportunity to meet target tissues during long circulation time. Indeed, cancer treatments with stealth immunoliposomes and transferrin-conjugated PEG-liposomes have been successful in animal models [7–9].

Abbreviations: DDS, drug delivery system; APRPG, Ala-Pro-Arg-Pro-Gly; GNGRG, Gly-Asn-Gly-Arg-Gly; ANET, antineovascular therapy; HUVECs, human umbilical vein endothelial cells; DOX, doxorubicin; PEG, polyethylene glycol; RES, reticuloendothelial system; EPR, enhanced permeability and retention; RGD, Arg-Gly-Asp; DSPC, distearoylphosphatidylcholine; EGM-2, endothelial cell growth medium-2; FBS, fetal bovine serum; ANOVA, analysis of variance; PEG-Lip, PEG-modified liposomes; PRP-PEG-Lip, APRPG-modified liposomes; NGR-PEG-Lip, GNGRG-modified liposomes; Dual-PEG-Lip, dual-targeting liposomes; PEG-DOX, DOX encapsulated in PEG-Lip; PRP-PEG-DOX, DOX encapsulated in PRP-PEG-Lip; NGR-PEG-DOX, DOX encapsulated in NGR-PEG-Lip; Dual-PEG-DOX, DOX encapsulated in Dual-PEG-Lip; EGFR, epidermal growth factor receptors; FR, folate receptors.

* Corresponding author. Tel.: +81 54 264 5701; fax: +81 54 264 5705.
E-mail address: oku@u-shizuoka-ken.ac.jp (N. Oku).

0304-3835/$ - see front matter © 2009 Elsevier Ireland Ltd. All rights reserved.
doi:10.1016/j.canlet.2009.06.008

Angiogenesis is a critical event for growth and hematogenous metastasis of tumors [10,11]. Therefore, antiangiogenic therapies are promised to suppress both tumor growth and metastasis [12,13]. Antineovascular therapy (ANET), one of antiangiogenic therapies, causes indirect tumor regression through damaging angiogenic vessels, which is achieved by delivering anticancer drugs to them with DDS technologies such as liposomes [14]. ANET could avoid the acquirement of drug resistance resulting from genetic or epigenetic mutation since this therapy targets angiogenic endothelial cells that are genetically stable [13]. The therapeutic effect of anticancer drugs would be amplified by targeting angiogenic cells since a large number of cancer cells are maintained by a relatively few endothelial cells for their survival and growth [15]. Furthermore, ANET is expected to have a broad anticancer spectrum since angiogenic vessels are necessary for all kinds of solid tumors.

We previously performed *in vivo* biopanning of a phage-displayed peptide library using an angiogenesis mouse model to identify a targeting-ligand for angiogenic vessel-specific drug delivery. As a result, Ala-Pro-Arg-Pro-Gly (APRPG) was identified as a novel peptide homing to angiogenic vessels [14,16]. Arap and coworkers injected phage-displayed peptide library into the circulation of human breast carcinoma-bearing mice and identified Asn-Gly-Arg (NGR) and Arg-Gly-Asp (RGD) motif [17]. NGR and RGD peptides motif bind selectively to CD13 (aminopeptidase N) and $\alpha_v\beta_3$ or $\alpha_v\beta_5$ integrins, respectively [18–20]. These peptides such as PRP, NGR and RGD were useful as targeting-ligands of liposomes since modification of liposomes with each of these peptides enhanced anticancer activity of DOX in tumor-bearing mice [21,22]. Until now, these peptides were used for angiogenic vessel-targeting individually and combinational effect of them has not been investigated. In the present study, we proposed a novel active-targeting strategy named "dual-targeting" in which two different kinds of targeting-ligands are modified on drug carriers. We hypothesized that two different ligands on the surface of liposomes might enable to enhance the potential of active-targeting cooperatively. We prepared dual-targeting liposomes modified with both APRPG and GNGRG and investigated the usefulness of them for ANET.

2. Materials and methods

2.1. Preparation of liposomes

All lipids were the products of Nippon Fine Chemical, Co. Ltd. (Takasago, Hyogo, Japan). Distearoylphosphatidylcholine (DSPC) and cholesterol with DSPE-PEG, DSPE-PEG-APRPG or DSPE-PEG-GNGRG (10:5:1 as a molar ratio), or with DSPE-PEG-APRPG and DSPE-PEG-GNGRG (10:5:0.5:0.5 as a molar ratio) were dissolved in chloroform/methanol, dried under reduced pressure, and stored *in vacuo* for at least 1 h. Liposomes were prepared by hydration of the thin lipid film with PBS, and frozen and thawed for three cycles using liquid nitrogen. Then, the liposomes were sized by extruding thrice through a polycarbonate membrane filter with 100 nm pores. Particle size and ζ-potential of the liposomes diluted with PBS were measured by use of a Zetasizer Nano ZS (MALVERN, Worcestershire UK, USA).

For an association study and a histochemical analysis, $DiIC_{18}$ (Molecular Probes Inc., Eugene, OR, USA) was added to the initial chloroform/methanol solution at a dose of 5 mol% of DSPC. For a biodistribution study, a trace amount of [^{3}H]cholesteryl hexadecyl ether (GE Healthcare UK Ltd., Buckinghamshire, England) was added to the initial solution. For a cell proliferation assay and a therapeutic experiment, DOX-encapsulated liposomes were prepared by a modification of the remote-loading method as described previously [23]. The encapsulation efficiency of DOX into the liposomes was more than 90% throughout the experiment. The concentration of DOX was determined by an absorbance at 484 nm.

2.2. Association of liposomes to HUVECs

Human umbilical vein endothelial cells (HUVECs, 2×10^4 cells/well) were seeded on gelatin-coated 24-well plate and cultured in endothelial cell growth medium-2 (EGM-2, Cambrex Bio Science Walkersville, Walkersville, MD) for 48 h at 37 °C in a 5% CO_2 incubator. Then, $DiIC_{18}$-labeled liposomes were added (final 0.05 or 0.1 mM as DSPC concentration) and incubated for 4 h at 37 °C. After washing these cells with ice-cold PBS, they were solubilized in 0.1% sodiumdodecylsulfate-containing 10 mM Tris buffer (pH 7.4). The amount of $DiIC_{18}$-labeled liposomes transferred to HUVECs was fluorometrically determined at an excitation wavelength of 549 nm and an emission wavelength of 592 nm by Infinite M200 (Tecan, Grödig, Austria). The amount of proteins in the samples was determined by bicinchoninic acid (BCA) protein assay (Pierce Chemical, IL). The amount of liposomes transferred into HUVECs was corrected by the amount of cellular proteins.

2.3. Cell proliferation assay

HUVECs (5×10^3 cells/well) were seeded on gelatin-coated 96-well plate and cultured in EGM-2 overnight at 37 °C in a 5% CO_2 incubator. Then, DOX or DOX-encapsulated liposomes were added (final 10 μg/ml as a dose of DOX) and incubated for 30 min at 37 °C. After washing these cells with PBS, they were cultured in EGM-2 for 48 h. Then, the growth of these cells was evaluated by a modified MTT assay using TetraColor One™ (Seikagaku, Tokyo, Japan).

2.4. Biodistribution study

Colon26 NL-17 cells were cultured in DME/Ham's F12 medium (WAKO, Osaka, Japan) supplemented with streptomycin (100 μg/ml), penicillin (100 units/ml), and 10% fetal bovine serum (FBS) at 37 °C in 5% CO_2. After harvesting of these cells, 1.0×10^6 cells were implanted subcutaneously into the posterior flank of 4-week-old BALB/c male mice (Japan SLC Inc., Shizuoka, Japan). The biodistribution study was performed at day 11 after tumor implantation. Size-matched Colon26 NL-17-bearing mice ($n = 5$) were injected with the radiolabeled liposomes *via* a tail vein (74 kBq/mouse). Twenty-four hours after the injection, the mice

were sacrificed under deep anesthesia for collection of the blood. The plasma was obtained by centrifugation (600g for 5 min). Then the heart, lung, liver, spleen, kidney and tumor were removed, washed with saline, and weighed. The radioactivity in each organ was determined with a liquid scintillation counter (Aloka LSC-3100). Distribution data are presented as % dose per 100 mg tissue. The total amount in the plasma was calculated based on the body weight of mice, where the plasma volume was assumed to be 4.27% of the body weight based on the data of total blood volume [23]. The animals were cared for according to the animal facility guidelines of the University of Shizuoka.

2.5. Intratumoral localization of liposomes

Colon26 NL-17 cells (1.0×10^6 cells/mouse) were inoculated as described above. DiI-labeled liposomes were administered *via* a tail vein of the mice at 10 days after tumor implantation. At 3 h after injection of the liposomes, the mice were sacrificed under deep anesthesia, and the tumors were dissected. The tumor tissues were embedded in optimal cutting temperature compound (Sakura Finetech, Co. Ltd., Tokyo, Japan) and frozen at −80 °C. Tumor sections (10 μm) were prepared with cryostat microtome (HM 505E, Microm, Walldorf, Germany), mounted on MAS-coated slides (Matsunami Glass Ind., Ltd., Japan), air-dried for 1 h, and washed twice with PBS. Endogenous avidin activity was blocked with a blocking reagent kit (Vector Laboratories, CA). After these sections had been blocked with 1% BSA in PBS, they were incubated with biotinylated anti-mouse CD31 rat monoclonal antibody (Becton Dickinson Lab., Franklin Lakes, NJ) for 18 h at 4 °C and then visualized after incubation with streptavidin-Alexa fluor 488 conjugates (Molecular Probes Inc., Eugene, OR) for 30 min at room temperature in a humid chamber. Then, the sections were mounted with Perma Fluor Aqueous Mounting Medium (Thermo Shandon, PA) and fluorescently observed with the LSM 510 META confocal microscope (Carl Zeiss, Co. Ltd., Germany).

2.6. Therapeutic experiment

Colon26 NL-17 cells (1.0×10^6 cells/mouse) were inoculated as described above. DOX-encapsulated liposomes or PBS were administered intravenously into the tumor-bearing mice ($n = 5$) at day 8, 11, 14 and 17 after the tumor inoculation. The treatment was started when the tumor volumes had reached about 0.1 cm^3. The injected dose of DOX in each administration was 3 mg/kg (about 0.05 mmol/kg as a dose of DSPC in liposomal formulations). The size of the tumors and the body weight of each mouse were monitored. Two bisecting diameters of each tumor were measured with slide calipers to determine the tumor volume. Calculation of the tumor volume was performed using the formula $0.4 \times (a \times b^2)$, where a is the largest and b is the smallest diameter.

2.7. Statistical analysis

Differences in a group were evaluated by an analysis of variance (ANOVA) with the Tukey *post hoc* test.

3. Results

3.1. Characteristics of dual-targeting liposomes

Particle size and ζ-potential of liposomes were determined. All kinds of liposomes used in the following experiments had the size of 110–150 nm in diameter and slightly negative charges (Table 1).

3.2. Affinity of dual-targeting liposomes to proliferative endothelial cells

To investigate whether dual-targeting liposomes (Dual-PEG-Lip) have more potent affinity to angiogenic vessels compared with APRPG-PEG-modified or GNGRG-PEG-modified single-targeting liposomes (PRP-PEG-Lip or NGR-PEG-Lip), the association of dual-targeting liposomes to HUVECs stimulated with proangiogenic cytokines were determined (Fig. 1). As a result, all liposomes modified with targeting-peptides were significantly associated to HUVECs compared with PEG-modified liposomes (PEG-Lip) in a dose dependent manner. Moreover, the association amount of Dual-PEG-Lip to HUVECs was significantly higher than that of PRP-PEG-Lip and NGR-PEG-Lip.

3.3. Effect of DOX encapsulated in dual-targeting liposomes on the growth of HUVECs

Anti-proliferative effect of DOX encapsulated in dual-targeting liposomes (Dual-PEG-DOX) on HUVECs was determined (Fig. 2). DOX encapsulated in all targeting-liposomes tested (PRP-PEG-Lip containing DOX, PRP-PEG-DOX; NGR-PEG-Lip containing DOX, NGR-PEG-DOX; and Dual-

Table 1
Particle size and ζ-potential of liposomes.

	Particle size (nm)	ζ-Potential (mV)
PEG-Lip	121.6 ± 11.7	−3.1 ± 0.9
PRP-PEG-Lip	124.8 ± 21.4	−3.1 ± 0.6
NGR-PEG-Lip	122.7 ± 22.4	−2.3 ± 0.9
Dual-PEG-Lip	116.2 ± 9.7	−2.9 ± 0.8
PEG-DOX	145.7 ± 16.2	−1.2 ± 0.6
PRP-PEG-DOX	143.7 ± 28.4	−2.0 ± 0.3
NGR-PEG-DOX	145.0 ± 44.4	−2.0 ± 0.3
Dual-PEG-DOX	136.7 ± 34.0	−2.8 ± 1.6

Parameters represent the mean ± SD.

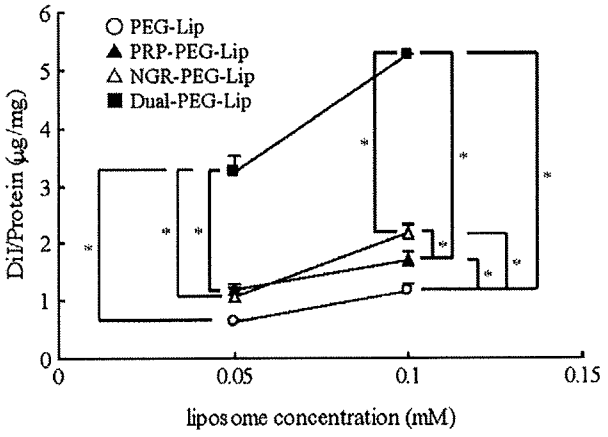

Fig. 1. The association of Dual-PEG-Lip to proliferating HUVECs. HUVECs were cultured in EGM-2 for 48 h, then added the indicated dose of $DiIC_{18}$-labeled liposomes and incubated for 4 h at 37 °C. After washing, the amount of liposomes associated to HUVECs was determined fluorometrically. Liposomes associated to HUVECs were represented as amount of $DiIC_{18}$ per cellular protein amount. Open circles, PEG-Lip; closed triangles, PRP-PEG-Lip; open triangles, NGR-PEG-Lip; and closed squares, Dual-PEG-Lip. Data show the mean value and SD. Significant differences are shown with asterisks (*$P < 0.01$).

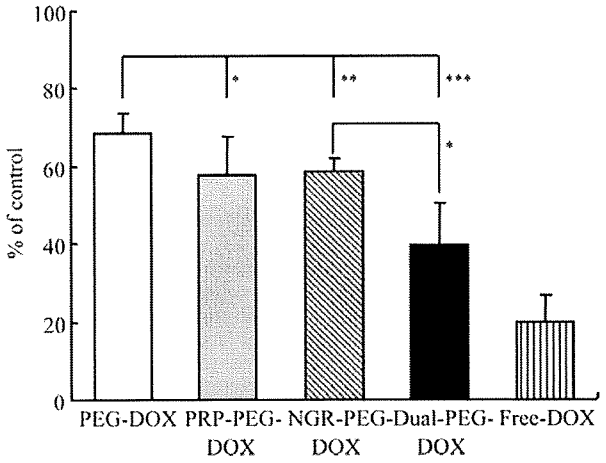

Fig. 2. Anti-proliferative effect of Dual-PEG-DOX on proliferating HUVECs. HUVECs were cultured in EGM-2 overnight. Then, DOX or DOX encapsulated in the liposomes were added (final concentration of 10 μg/ml as a DOX dosage) and incubated for 30 min at 37 °C. After 48 h incubation, cell growth was determined by modified MTT assay using TetraColor One™. Data represent the anti-proliferative effects of each sample as percent of control and SD. Open bar, PEG-DOX; grey bar, PRP-PEG-DOX; hatched bar, NGR-PEG-DOX; closed bar, Dual-PEG-DOX; and stripe bar, Free-DOX. Asterisks indicate the significant differences: $^{*}P < 0.05$, $^{**}P < 0.01$ and $^{***}P < 0.001$.

PEG-DOX) significantly suppressed the growth of HUVECs compared with DOX encapsulated in PEG-Lip (PEG-DOX). Furthermore, the antiproliferative effect of Dual-PEG-DOX was significantly higher than that of NGR-PEG-DOX and tended to be high compared with that of PRP-PEG-DOX. These anti-proliferative effects were observed in a dose dependent manner (Supplemental data).

3.4. Biodistribution of dual-targeting liposomes

The biodistribution of the liposomes was determined in Colon26 NL-17 carcinoma-bearing mice (Fig. 3). NGR-PEG-Lip tended to accumulate in the spleen. In contrast, the accumulation of PRP-PEG-Lip in the spleen

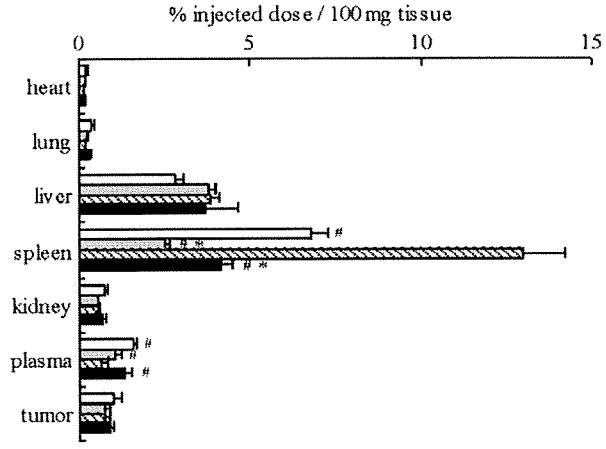

Fig. 3. Biodistribution of Dual-PEG-Lip in the tumor-bearing mice. Size-matched Colon26 NL-17-bearing mice ($n = 5$) were injected with radio-labeled liposomes *via* a tail vein. Twenty-four hours after injection, the radioactivity in each organ was determined. Data are presented as percent of the injected dose per 100 mg tissue and SD. Open bar, PEG-Lip; grey bar, PRP-PEG-Lip; hatched bar, NGR-PEG-Lip; and closed bar, Dual-PEG-Lip. Significant differences are shown with asterisks (versus PEG-Lip): $^{*}P < 0.01$, and sharps (versus NGR-PEG-Lip): $^{\#}P < 0.01$.

was lower than PEG-Lip. Interestingly, Dual-PEG-Lip did not accumulate in the spleen although it contains a half amount of GNGRG peptides in comparison to NGR-PEG-Lip. The amount of NGR-PEG-Lip in the plasma was significantly lower than other liposomes tested. On the other hand, Dual-PEG-Lip showed a long-circulating property like PEG-Lip and PRP-PEG-Lip. The accumulation in the tumor was similar level among all liposomes tested.

3.5. Intratumoral localization of dual-targeting liposomes

Intratumoral localization of the liposomes was determined in the tumor syngrafts to evaluate the affinity of Dual-PEG-Lip to angiogenic vessels *in vivo* (Fig. 4). As shown in Fig. 4a–c, PEG-Lip was observed around tumor angiogenic vessels, indicating that it extravasated from these vessels. On the other hand, PRP-PEG-Lip (Fig. 4d–f), NGR-PEG-Lip (Fig. 4g–i) and Dual-PEG-Lip (Fig. 4j–l) localized on angiogenic vessels. In addition, Dual-PEG-Lip localized on angiogenic vessels more intensely than PRP-PEG-Lip and NGR-PEG-Lip.

3.6. Therapeutic effect of DOX encapsulated in dual-targeting liposomes

The therapeutic effect of Dual-PEG-DOX against the solid tumor was examined (Fig. 5). The body weight change was not observed in all groups tested (data not shown). As shown in the figure, significant differences in the tumor volume were observed between liposomal DOX-treated group (PEG-DOX, PRP-PEG-DOX, NGR-PEG-DOX or Dual-PEG-DOX) and control group 24 days after tumor implantation. Antitumor effect of Dual-PEG-DOX was the highest among all liposomal formulations. Dual-PEG-DOX significantly suppressed the tumor growth in comparison to PEG-DOX.

4. Discussion

In the present study, we proposed a novel targeting strategy, "dual-targeting", and applied it to ANET. We firstly determined the affinity of liposomes modified with two different targeting peptides (namely APRPG and GNGRG) to proliferating HUVECs as an *in vitro* model of angiogenic endothelial cells. As a result, Dual-PEG-Lip showed the highest affinity to proliferating HUVECs dose-dependently. This data suggests that two different kinds of angiogenic vessel-targeting peptides on the liposomal surface cooperatively enhanced the association of these liposomes to proliferating HUVECs. Saul et al. previously reported that liposomes targeting epidermal growth factor receptors (EGFR) and folate receptors (FR) improved selectivity to target cells compared with single-ligand liposomes [24]. Although these liposomes attenuated non-specific binding to non-target cells, the affinity of them to target cells was not determined. In contrast, our data provided the evidence that dual-targeting achieved enhancement of the targeting activity. In fact, Dual-PEG-DOX suppressed the growth of proliferating HUVECs in comparison to non-targeting or single-targeting liposomal DOX, reflecting that Dual-PEG-Lip showed the highest affinity to proliferating HUVECs.

Previous study showed that liposomes modified with NGR accumulated in the spleen after intravenous injection [22]. Our data also indicated that NGR-PEG-Lip tended to accumulate in the spleen. However, this wrong property caused by NGR was improved in Dual-PEG-Lip administration group. Consequently, Dual-PEG-Lip remained in the plasma more than NGR-PEG-Lip. These results might be related to the amount of peptide on the liposome surface although precise mechanism is not cleared at present. There were no statistical differences in the accumulation